


RESEARCH

Open Access



# Development of eco-friendly brake pads using industrial and agro-waste materials

Joseph O. Dirisu<sup>1\*</sup> , Imhade P. Okokpujie<sup>2,3\*</sup>, Pepple B. Apiafi<sup>1</sup>, Sunday O. Oyedepo<sup>1</sup>, Lagouge K. Tartibu<sup>2</sup>, Olugbenga A. Omotosho<sup>1</sup>, Emmanuel O. Ogunkolati<sup>1</sup>, Enoch O. Oyeyemi<sup>1</sup> and John O. Uwaishe<sup>1</sup>

\*Correspondence:

joseph.dirisu@covenantuniversity.edu.ng; ip.okokpujie@abuad.edu.ng

<sup>1</sup> Department of Mechanical Engineering, Covenant University, Ota, Nigeria  
<sup>2</sup> Department of Mechanical and Industrial Engineering Technology, University of Johannesburg, Johannesburg 2028, South Africa  
<sup>3</sup> Department of Mechanical and Mechatronics Engineering, Afe Babalola University, Ado Ekiti, Nigeria

## Abstract

There has been an increase in research over the past decades into the use of environmentally friendly materials in brake pads, such as natural fibres. This is due to the possibility that natural fibbers could serve as an alternative to the noxious asbestos materials in tribological applications like brake pads. As a result, utilizing the compacting mould technique, an asbestos-free friction material was developed using agricultural waste (coconut shell and oil bean stalk) as a filler element, alongside aluminium dross, metal chip industrial wastes and carbon black. The filler material considered had particles as small as 300  $\mu\text{m}$ , with epoxy resin serving as the binding agent. Using these waste materials can help reduce environmental pollution and the risk to animal and plant life (Preeti et al., *Pharma Innov J* 7:94–102, 2018; Sajib, A Study on the effects of environmental pollution on human life in the riverbank area of Barishal City Corporation (Kirtankhola River), 2021). This research aimed to replace asbestos in brake pads due to its carcinogenic nature, reducing the health risks associated with manufacturing and using these brake pads. The brake pad materials were cast and produced using square wooden moulds. Four samples were created, comprising the same mixing ratio but varying in reinforcement fibre and particle size, with epoxy resin used as the matrix. Various tests were conducted on these samples, including a water absorption test, specific gravity test, compressive strength test, hardness test, thermal conductivity, SEM and EDX. The developed brake pads underwent microscopic characterization and structural examination using a scanning electron microscope (SEM) fitted with energy-dispersive X-ray spectroscopy (EDX) for elemental characterization. Thermal conductivity was obtained using automated Lee's Disc apparatus. Comprehensive strength analysis was conducted using a universal testing machine (UTM).

The specific gravity tests yielded values for the developed composites in the range of 1.136–1.257, while the commercial brake pad had a value of 2.081, indicating that the produced samples were lighter and less dense. The water absorptivity of the developed samples ranged from 0.95 to 2.174%, while the commercial brake pad had a value of 1.031%. For the hardness tests, at three different loads, the developed values ranged from 16.4HV3 to 19.4 HV3; 26.4HV30 to 28.7HV30; and 25.5HV100 to 29.6HV100, while the commercial brake pad had values of 16.5HV3, 28.4HV30 and 28.2HV100.

Sample C (212  $\mu\text{m}$ : coconut shell powder) exhibited the most desirable characteristics with five values: water absorptivity 0.95, compressive strength 120.5 MPa, hardness value 29.6 HV100, wear resistance 0.099 mm/mm<sup>3</sup>, specific wear rate 1.00 mm<sup>3</sup>/Nm. The outstanding values were attributed to the chemical composition, particle sizes and good interfacial bonding of the microstructure.

The developed brake pads performed favourably when compared with the existing commercial brake pads. The chemical tests showed that the natural fibres bonded well with the epoxy matrix. The thermal and mechanical tests yielded comparable results with the values obtained from the commercial brake pads. Therefore, the developed materials for brake pads can be considered suitable replacements for asbestos brake pads.

**Keywords:** Brake pad, Composite material, Comprehensive strength, Eco-friendly material, Hardness, Natural fibre, Thermal conductivity, Water absorptivity

## Introduction

In ancient times, the amount of waste produced by humans was never a threat to human life and the ecosystem due to lower population densities and the fact that most natural resources that constitute waste today (such as metals, fossil fuels) were either undiscovered or used in very minimal quantities. Tools and weapons made of metals and wood were used for extended periods before disposal and often handed down to younger generations. Nowadays, the significant waste generated includes ashes and human biodegradable waste (faeces, corpses, etc.) [51]. Waste refers to any material unused and rejected as worthless or unwanted. As more natural resources are exploited and used, they leave behind a substantial amount of waste products, posing a significant problem in their disposal. Recycling has emerged as a solution, reusing waste materials to create new valuable materials, thus reducing the amount of waste generated [16, 61].

Human activities have led to pollution in our immediate surroundings; one common form is nitrogen pollution [116]. Dispersed by air, it affects not only the air but also land and water. When fossil fuels burn, hydrocarbons ideally burn in the air, forming carbon dioxide, water and nitrogen gas. However, incomplete combustion results in the formation of carbon monoxide and nitrogen oxides, which have adverse effects, including acid rain and smog. Nitrogen pollution mainly occurs in the form of nitrogen oxides, with some coming from ammonia, mainly due to agricultural activities and the combustion of fossil fuels [44]. This abundance of nitrogen in the air is transferred to the land, then to water bodies, leading to pollution, algal blooms, low oxygen areas, low pH and excess ammonia, harming marine life and potentially leading to extinction. Nitrogen makes up 77% by mass and 79% by volume of the air, playing a crucial role in the survival of plants and animals. Primary sources of nitrogen pollution include automobiles, power plants, industrial operations and large engines like those on ships, aircraft and locomotives [5, 57]. Some solutions to this problem involve reducing emissions through various means, such as using catalytic converters in automobiles and adopting renewable and clean energy sources [86, 107].

Other steps to reduce pollution include decreasing carbon footprints, lowering greenhouse gas emissions and promoting recycling [3]. A carbon footprint quantifies how much greenhouse gas, mainly carbon dioxide, is released into the surroundings

by any activity or process. In the past, chlorofluorocarbons were used in refrigerants but were found to have adverse greenhouse effects, contributing to ozone layer depletion, and were replaced by safer compounds [28]. Similarly, asbestos was discovered to cause severe health challenges (such as cancer and respiratory diseases) in individuals exposed to it, including those using it in manufacturing other products or residing in homes built with asbestos. Asbestos is a significant component in automobile brake pads. The search for materials that can perform equally or better under similar conditions while posing minimal or no harm to human life led to the discovery and use of natural fibres [93]. As the world moves towards a greener approach, more industries are moving away from harmful substances, turning towards using industrial or agricultural waste for various functions, including structural reinforcement and binding.

Some materials, when combined and used, prevent waste from harming the environment. Phenolic composites, due to their high coefficient of friction, reduced wear at room temperature and ability to withstand temperatures up to 250°C, find extensive use in automotive brake pads. When developing environmentally friendly brake pads, they can accommodate organic ingredients instead of harmful ones. These composites have been studied for mechanical applications due to their excellent bonding with other agro-industrial waste materials. Extensive research has been conducted on phenol-based composites containing various elements such as fly ash, bagasse ash, palm kernel fibres, coconut shell, barium sulfate, oil bean stalk, basalt, flax, shells, alumina, titanium dioxide, crushed metal chips and zirconium dioxide [33, 55, 78, 80]. Friction compounds based on phenolic resin usually have limited tribological use due to their generally low stability and wear resistance. To improve these properties, several elements like abrasives, binders, fillers, friction modifiers (solid lubricants) and reinforcing fibres are added [97]. Asbestos has been replaced by various fibres such as metallic, glass, ceramic and carbon fibres [43]. Among these, low-carbon steel is widely used as a metallic fibre due to its exceptional heat stability. Ceramic materials, composed of silica and alumina, also improve wear resistance, insulating properties and high-temperature performance [32, 34, 49]. The addition of different fibres can lead to diverse behaviours in semi-metallic friction materials concerning tribology. To enhance wear resistance, thermal stability and strength, metallic components are often used in friction materials. Metals like copper, steel, iron, brass, bronze and aluminium have been utilized as fibres or particles in friction substances. The friction and wear of these materials are influenced by the type, shape and hardness of the metallic components [49]. Selecting these materials and their proportions carefully results in various mechanical properties, including the coefficient of friction, wear rate and compressive strength, among others. These desirable properties enable research and development engineers to choose eco-friendly materials for brake pad and brake lining production [17–19, 90, 91].

This research aims to develop an eco-friendly brake pad using natural fibres from waste materials, focusing on enhancing performance variables. The study intends to manufacture eco-friendly brake pads using natural fibres; conduct mechanical, chemical and thermal tests on these brake pads; and compare the test results with those obtained from existing brake pads. The production of these eco-friendly brake pads will help mitigate the health risks posed by asbestos in conventional brake pads. This research seeks to utilize

agricultural and industrial waste as a means of solid waste management, while also serving as a means of recovering wealth from waste materials. Furthermore, it promotes the establishment of sustainable small-scale businesses, contributing to national economic advancement. The study involves testing and characterizing a standard automobile brake pad, manufacturing, testing and characterizing an eco-friendly brake pad made from natural fibres, and ultimately comparing the performance of the two brake pads.

**Solid waste management**

Kaza et al. [54] claim that by 2050 waste generation will significantly surpass population growth, more than doubling. Although solid waste management is evolving and improving worldwide, there is still much work to be done. Improper waste management negatively impacts everyone, but it disproportionately affects the most vulnerable members of society [47, 56]. These individuals lose their lives and homes due to waste dump landslides, work in hazardous conditions while collecting waste, and suffer severe health effects. Moreover, the environment frequently bears a heavy toll. In 2016, worldwide production of plastic waste amounted to 242 million tonnes, constituting 12% of all municipal solid waste [102, 104]. Despite the increasing consumption of plastics, plastic waste is suffocating our oceans. The lack of adequate infrastructure to manage the evolving waste composition is leading to rapid growth in waste for residents, cities and nations. Furthermore, it was estimated that in 2016, solid waste management contributed to 1.6 billion tonnes of carbon dioxide equivalent (CO<sub>2</sub>-equivalent) greenhouse gas emissions, accounting for approximately 5% of global emissions. If the industry does not make improvements, it is projected that by 2050, solid waste-related emissions will reach 2.6 billion tonnes of CO<sub>2</sub>-equivalent. The historic Paris Agreement of 2017 saw more than 80 nations pledge to reduce emissions, and one way to support this endeavour is through enhancing waste management.

Figure 1 illustrates the waste generated per region. The data highlights the environmental threat posed by waste if not recycled. From Fig. 2, it is evident that industrial

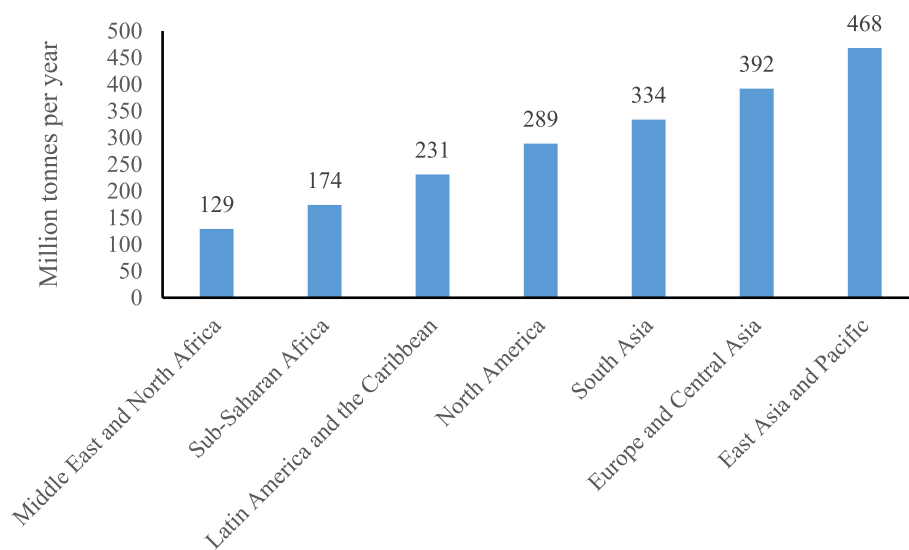


**Fig. 1** Waste generation by region [54]

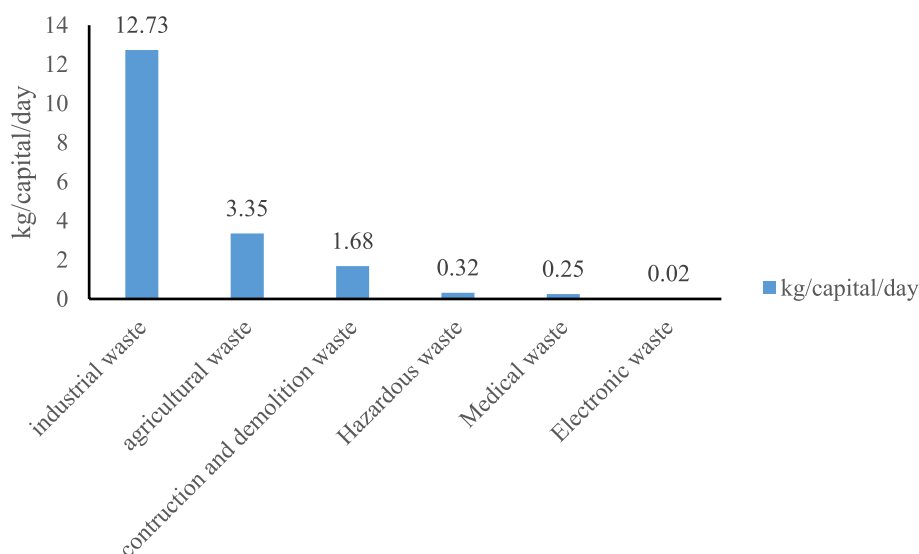


**Fig. 2** Global average special waste generation [54]

waste ranks the highest. Implementing an efficient waste conversion system is crucial to reduce the amount of waste occupying land, thus mitigating the threat to the ecosystem [106].

Solid waste management, as the term suggests, involves the collection and processing of solid waste materials. Since humans transitioned from a nomadic lifestyle to establishing communities, solid waste has been an escalating issue, especially with the advent of industrialization. Every item has a lifespan during which it serves a purpose, and once it exceeds that time frame, it is disposed of and becomes waste [27, 98]. Solid waste management aims to regulate the disposal of these items to reduce pollution and prevent the spread of diseases. Waste can be classified into various categories, including organic and inorganic waste, combustible and non-combustible waste, toxic and hazardous waste, carcasses, ashes, construction waste and recyclable waste. These different types of waste decompose at varying rates, ranging from a few days to millions of years, such as in the case of glass and plastics. The most common disposal method is through open landfills, which emit unpleasant odours and contaminate the air in their immediate vicinity. Sometimes, the waste can seep into nearby water bodies, leading to water pollution [37, 66].

The waste deposited here is sourced from varying locations, and some of them are listed below [38]:

*Residential:* (e.g. homes) mostly organic, combustible, ashes and recyclable wastes.

*Industrial:* (e.g. factories, plants, construction sites) organic, combustible, non-combustible, toxic, ashes and construction wastes.

*Commercial:* (e.g. hotels, office buildings) mostly organic, combustible, recyclable and some hazardous wastes [70, 71].

*Institutional:* (e.g. schools, prisons, government centres) organic, recyclable, non-recyclable, combustible and hazardous wastes.

*Construction:* (e.g. construction sites) construction, recyclable, non-recyclable, combustible, non-combustible and hazardous wastes [59].

*Municipal services:* (e.g. streets, parks, beaches) organic, combustible and recyclable wastes.

*Treatment plants and sites:* (e.g. mines, refineries) construction, non-recyclable, toxic, combustible and non-combustible wastes [69].

*Agricultural:* (e.g. vineyards, orchards, dairies) organic, combustible, toxic and recyclable wastes.

*Biomedical:* (e.g. hospitals) carcasses, organic, combustible, toxic and recyclable wastes [68].

How solid waste materials are disposed of can affect the quality of human life and the environment, ranging from minimal to devastating [24–26]. Some of the effects of improper solid waste handling [1] include:

*Untidy environment:* improper handling of municipal waste will lead to untidy streets and public areas.

*Human health:* people living close to landfills and primarily those working on those sites are exposed to various health risks and conditions, including cutaneous infections, respiratory issues and even cancers, tumours, or reproductive issues if exposed to toxic materials.

*Pathogens:* these unsanitary grounds attract disease-causing and carrying organisms that dwell and breed there before spreading diseases.

*Environmental pollution:* Toxic and hazardous waste can affect soil fertility and seep into and contaminate the ground water.

*Effect on animal life:* animals grazing near toxic soil from landfills can be poisoned, and marine life can be compromised if the waste gets into water bodies.

*Toxic gas emission:* When some hazardous chemicals are absorbed by non-toxic combustible materials like paper and are burned, they form toxic gases that are dangerous to human life [75, 79, 89, 108].

The landfill method of solid waste management is inadequate and highly unsanitary. There are various methods available for improving the landfill method of managing solid waste, including sanitary landfills, incineration, composting, pyrolysis, recovery and recycling. Among these methods, recycling stands out as the most efficient approach, generating minimal waste material or by-products. Essentially, recycling involves finding alternative uses for materials, thus extending their lifespan [67]. Figure 3 illustrates methods for converting waste, thereby generating wealth. Waste materials are commonly used in the development of various composites for brake pads and other products. These composites incorporate materials like slags, metal chips and aluminium dross from industrial waste, as well as banana peels or coconut shells from agricultural waste, which are combined with other waste materials to create eco-friendly products [63, 64, 96, 99, 109, 111–113].

### **Review of recent work on brake pad materials**

Brake pads are essential components of all automobiles equipped with braking discs. These pads undergo rigorous testing to determine the characteristics necessary for their specific application. Properties such as abrasion resistance, friction coefficient, hardness,

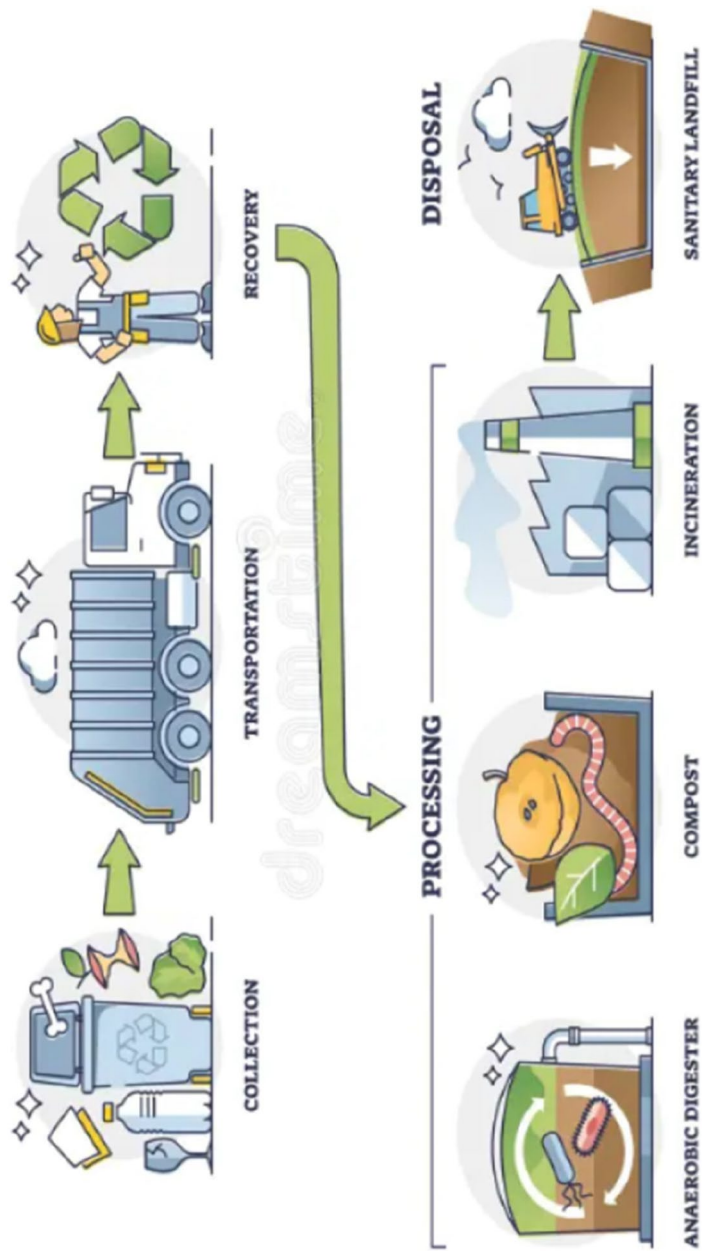


**Fig. 3** Solid waste management. Source: <https://vectorsmine.com/item/solid-waste-management-steps-with-processing-and-disposal-outline-diagram/>



tensile strength, specific gravity, compressive strength, oil absorption, water absorption, thermal conductivity, disc temperature and stopping time are commonly evaluated to assess brake pad viability [73, 100]. As vehicles become faster, it is increasingly important to find effective ways to decelerate them quickly. Brake systems play a crucial role in preventing accidents, safeguarding lives and protecting property from damage, making them indispensable components in any automobile [45, 94]. Friction brakes function by converting a moving vehicle's kinetic energy into heat through friction, subsequently dissipating this heat to the surroundings to slow down the vehicle [46]. With higher speeds, materials with higher friction coefficients are required to slow down the vehicle efficiently (reduce response time). Moreover, due to the increased kinetic energy being converted to heat, materials with good thermal conductivity and high melting points are preferable. Effective heat dissipation materials are also necessary. Other desirable brake pad qualities include low wear rates, resistance to corrosion, low water absorption, light weight, durability, minimal noise and reasonable cost [84, 85].

Two primary types of friction brakes are drum brakes and disc brakes. Initially, drum brakes were widely used, but the transition to disc brakes occurred because of their superior braking performance, especially in heavier vehicles [45]. Disc brakes dissipate heat more effectively than drum brakes and exhibit lower wear rates, hence their widespread adoption. Brake pads consist of various materials serving different functions, including abrasives, friction modifiers, fillers, reinforcement agents and binders [58]. Some materials serve multiple functions, one of which historically was asbestos. However, asbestos has adverse health effects, causing lung-related illnesses when its fibres are inhaled. Due to its carcinogenic nature, it has been banned in many applications, necessitating the exploration of alternative materials. Researchers have investigated utilizing industrial and agricultural waste products for brake pad production [2, 42, 95]. Agricultural wastes, including cocoa bean shells, eggshells, coconut shells, banana peels, periwinkle shells, palm kernel shells, maize husks, rice husks and bagasse, are primarily used as filler materials and particulate reinforcements. They are cost-effective and contribute to waste reduction and recycling efforts [36, 50]. Industrial waste is utilized for friction production and modification, sourcing materials such as factory waste, foundry slag and machine shop chips. This practice aids in conserving metal natural deposits and repurposes materials typically classified as waste [39, 41, 110].

Asbestos's presence in brake pads poses significant health risks due to its carcinogenic nature. It is imperative to develop eco-friendly alternatives with improved operational performance while posing minimal health risks. Moreover, there is a growing issue of solid waste accumulating in landfills, necessitating the development of viable products from waste materials to reduce environmental hazards and protect natural water bodies. Reports from the World Bank in 2012 and 2018 projected significant increases in global solid waste production and associated management costs, particularly in developing countries. Numerous studies have explored creating asbestos-free brake pads using materials such as coconut shells and palm kernel shells (PKS). Researchers worldwide are focused on utilizing agricultural or industrial waste as raw materials, aiming for both financial benefits and environmental improvements. Asbestos was phased out due to its carcinogenic nature, although some existing uses are still allowed. The ban was initiated in 1989, but challenges in finding substitutes led to the 1991 relaxation of this



prohibition [8]. Studies like Bashar et al. [20] developed brake pads using coconut shells, iron chips, epoxy resin, methyl ethyl ketone peroxide, cobalt naphthenate, iron, silica and brass. The findings showed that increasing ground coconut powder amounts led to reduced strength and increased brittleness, similar to other research on polymer composites made from treated and untreated palm kernel nut shells [8, 21, 23, 88]. Banana peels were examined by Idris et al. as a replacement for asbestos in brake pad production using phenolic resin as the binder. Varying the resin content showed that higher resin percentages improved compressive strength, hardness and specific gravity while reducing burn, water soak and wear rates. Samples with 25% uncarbonized banana peels and 30% carbonized banana peels exhibited overall better properties [48, 65, 101, 114].

### **Materials and methods**

This section gives a detailed explanation of all the activities carried out during this research project work. All the processes undergone are outlined. Also, the materials used, the equipment and various apparatuses are discussed. Design dimensions, mixing ratios and the reasons specific equipment or processes were employed are also discussed.

#### **Materials**

The materials used in this research were locally sourced from nearby farms, markets and workshops. Aluminium dross was obtained from Aluminium Rolling Mill (ARM), Ogun Housing Estate, Ota, Ogun State. Oil beanstalks were obtained from the Covenant University grounds; coconut shells were obtained from a nearby farm, and metal chips were obtained from the CNC machine at the Mechanical Engineering Department of Covenant University. Carbon black, epoxy resin, and hardener were purchased from vendors in a nearby market. Aluminium dross served as the parent material, coconut shell, and oil beanstalk served as filler materials in their various samples, carbon powder was utilized as a lubricant, metal chips were employed as friction additives, and a mixture of epoxy resin and hardener functioned as the matrix and binder. These materials were selected because they show good bonding characteristics with the matrix material (epoxy resin). Including lubricants and friction, additives depended on the application, as braking requires contact and friction.

#### ***Coconut shell powder and aluminium dross powder***

The coconut shells, as shown in Fig. 4, were obtained from a nearby farm where they constituted a part of its waste materials. The coconut shell powder served as the reinforcement for the epoxy matrix and bonded with the aluminium dross. Coconut shell powder was used because past studies show that it exhibits a good interaction with epoxy.

Aluminium dross, as shown in Fig. 4, is a by-product of aluminium smelting process. Combined with epoxy, it can produce lightweight composites with good thermal and wear resistance. It is one of the filler materials and bonds with the natural fibres and carbon black in an epoxy resin matrix [29, 31, 62, 81, 103].

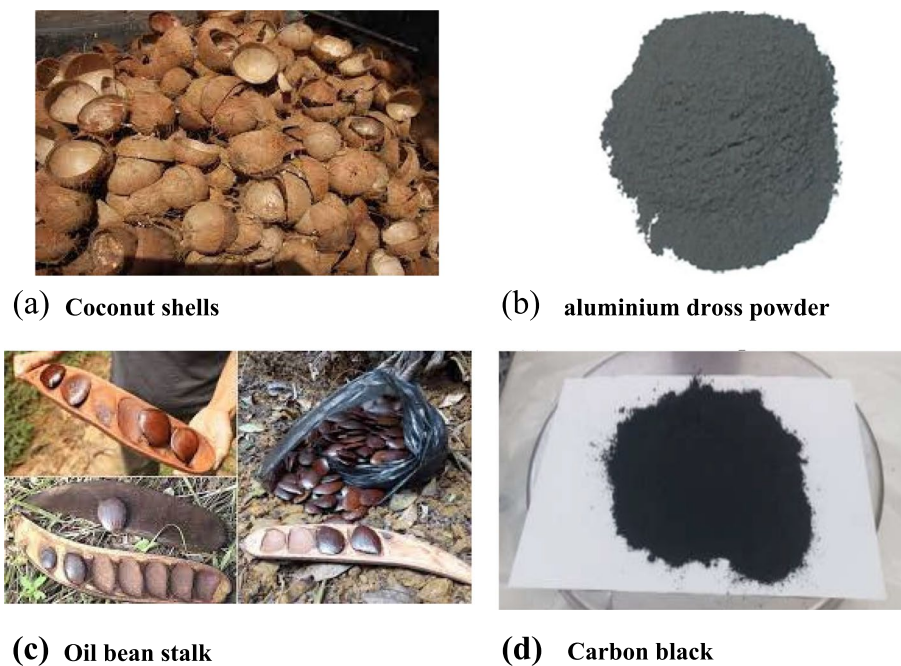


**Fig. 4** Coconut shell and aluminium dross powder

#### ***Epoxy resin, oil beanstalk, carbon black and metal chips***

Epoxy resins are a class of polymer that contains the epoxide group. These resins can be cross-linked (also known as curing) with themselves through hardeners (catalytic homopolymerization) or cross-linked with other reactants to form thermoset polymers [52, 105]. These polymers usually possess good thermal and chemical resistances and mechanical properties that can all be enhanced by adding reinforcement fibres to form thermoset polymer composites. Epoxy served as the matrix of the composite produced.

African oil bean (*pentaclethra macrophyllaa*) is a legume with medicinal value and high protein content. Its physical properties deem it feasible to be used as a reinforcement for a polymer composite. The oil beanstalk is the exocarp that protects and contains the oil bean seed. In this experiment, the oil beanstalk reinforces the epoxy matrix [29, 30].

It is obtained from the incomplete combustion of vegetables or petroleum products. It can be used as a reinforcement material as it increases tensile strength and wear resistance. Figure 4 also shows a pulverized carbon black. Chips are formed from metal removal processes; as the metal is cut, it flows in the form of chips. The metal chips used were obtained from the Mechanical Engineering Department, Covenant University CNC (computer numerical control) machine, as the chips were smaller than the chips available from the lathe and drilling machines. The chips were ground for further size reduction. Figure 5 shows pulverized metal chips. Coolant from machining was removed from the chips, and they were dried in the oven to remove moisture.

#### ***Apparatus***

This research used various equipment to provide automation, accuracy, measurement, mechanical force, heating, or testing. A few of them are shown in Fig. 5. The equipment



**Fig. 5** Material and apparatuses used

used in this project includes mould boxes, a digital weighing balance, sieves, sieve shakers, an oven, an abrasion machine, a ball mill, emery cloth, a hack saw, files and beakers. Some of the equipment used are discussed in this section. A sieve shaker is a machine that produces vibration to aid the separation of materials of different particle sizes. When sieves are used manually, a reciprocating motion is required for the particles to separate from each other and allow the smaller particles to pass through the mesh and into the receiver, leaving particles more significant than the stated mesh size. A sieve shaker provides a vibratory motion that separates these particles faster without requiring as much manual labour. It comprises a base plate where the receiver sits, the sieves are connected to the receiver, and the sieves are covered to prevent spillage of its content. It also has restraints to hold the sieves in place, which are of adjustable height and grip. The sieve shaker has a timer, a start and stop button and indicator lights. It is electrically powered and connected to a socket. This was used to reduce the particle sizes of the coconut shell and the oil beanstalk. This is accomplished by the impact and grinding action of colliding steel spheres in a rotating drum housing the materials to be grinded and the desired number of steel spheres. The equipment comprises a drum with an opening for loading the equipment, a cover with bolts for keeping the opening closed when in operation, a tray or catch pan for depositing the material after an operation, hardened steel balls of different sizes, an electric motor and chain drive for rotating the drum, a control panel for selecting the number of revolutions, a stop and start button and a plug that connects it to an electrical outlet.

An oven is a heating chamber that can be used for various processes such as removing moisture from materials to better their mechanical properties, sterilizing tools, heat treating materials and processing materials. The electric oven is an improvement over the traditional oven because it possesses a thermostat and an interlock switch. The oven

is used for heating, drying and baking materials by supplying dry heat by convection. It was used to remove moisture from the metal chips. It was selected because dry heat prevents rust build-up. This oven comprises a heating element, heating chamber, thermostat, interlock switch and adjustable temperature controls and sources its power from electricity [74]. This machine is used to determine the mass of an object, and it is accurate to 1 g. It has a digital display where a readout is shown the measured mass. The object to be measured is placed on a flat plate. When the mass of a powdered substance is to be determined, a piece of paper is placed on the plate, and then the scale is tared to zero instead of manually subtracting the weight of the paper. The machine is electrically powered and is connected to a socket outlet. It is also equipped with a power button and a tare button and can give values in either imperial or SI units. Some of the devices used in the research were handheld, mobile equipment such as a hacksaw, file, emery cloth, beakers and measuring cylinders. The hacksaw, file and emery cloth were used post-production for sizing and finishing the final product to be sent out for testing. The measuring cylinder and beakers were used to provide volumetric accuracy.

## **Methods**

The flow chart in Fig. 6 shows the methods to achieve this research.

### ***Collection and preparation of materials***

The materials were locally sourced from nearby farms, markets and workshops. They were sundried to remove moisture from them. The coconut shell, oil beanstalk, aluminium and carbon were put into a ball mill to be reduced to powder form; Fig. 7 shows the pulverized oil beanstalk and coconut shell.

The metal chips were obtained from the CNC machine at the Covenant University Mechanical Engineering Department. The metal chips had an oily feel due to the coolant used in machining, this was removed using sodium hydroxide, and the chips were then dried using an oven. Epoxy resin and hardener were purchased from a chemical store. The materials were then sieved using two different mesh sizes; 212 and 300  $\mu\text{m}$ . Each material was sieved using these two sizes and grouped accordingly. The sieving was carried out manually for the smaller sieve size and automatically for the larger sieve size with the aid of a sieve shaker.

### ***Composite preparation and sample composition***

Four samples were produced, which varied based on materials or particle size; see Table 1. The dry materials were first manually mixed thoroughly to achieve a homogeneous mixture for 10 min. The final mixture was then achieved by mixing the dry mixture thoroughly with the binder. Following that, this mixture is stirred at a high speed for 15 min with the resin-hardener mixture to create a magnetic stirrer. The various sample compositions are also listed in Table 1. The composition ratios were performed massively, and a digital weighing balance was used to measure the appropriate masses.

The binder is composed of epoxy resin and hardener. The two materials were mixed in a ratio of 2:1 with the epoxy in greater quantity. The binder was then mixed with

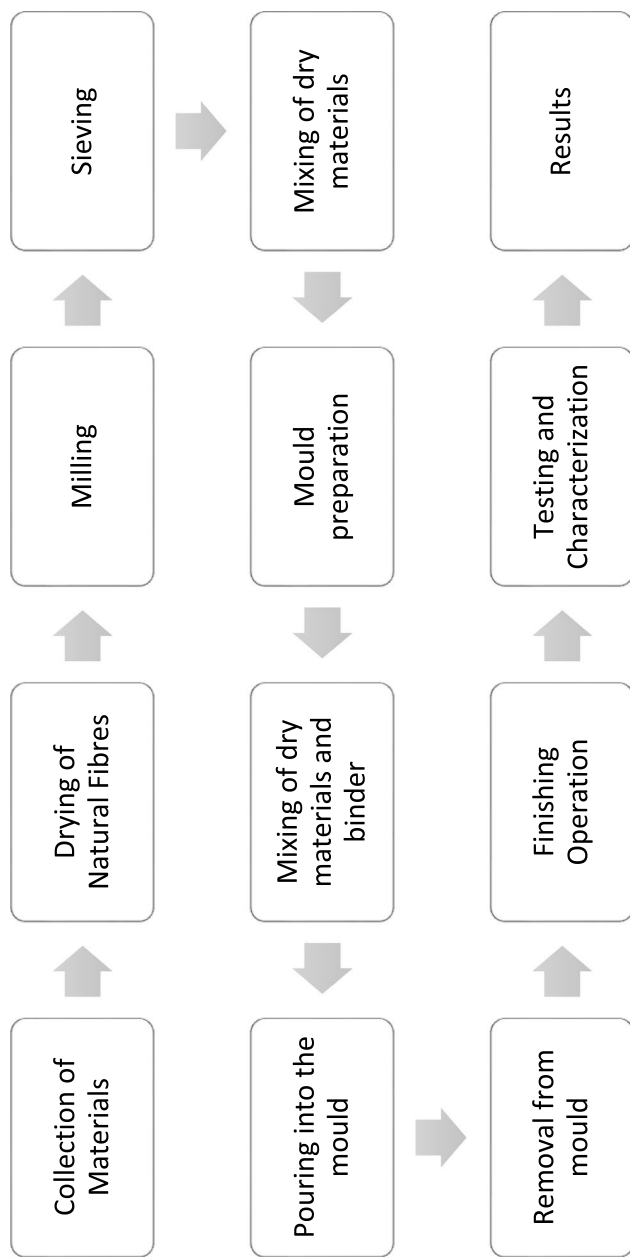
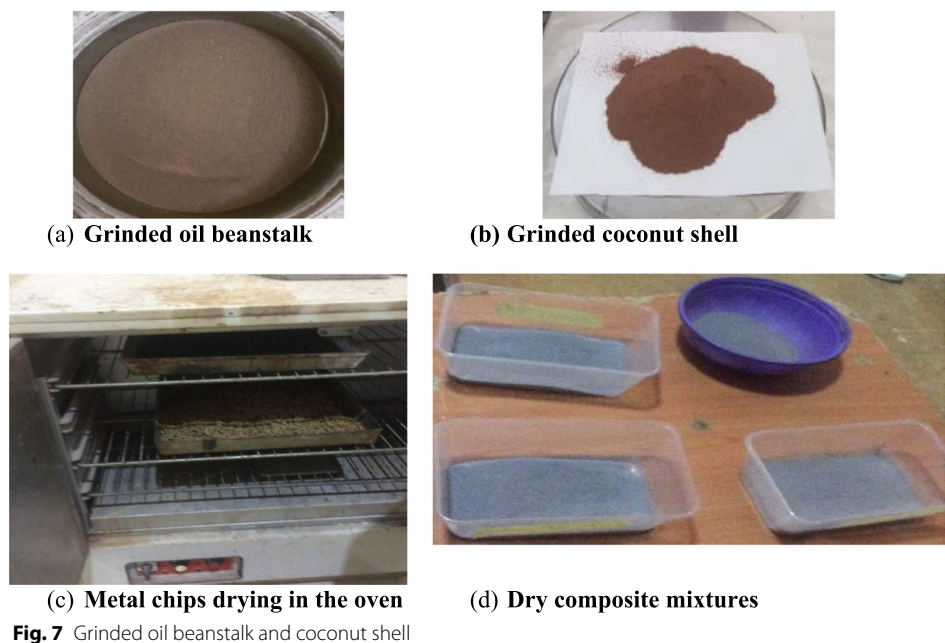


Fig. 6 Flow chart of mould production



the dry composite mix as shown in Table 2. The composition ratios for mixing the epoxy with the hardener and the binder with the dry mixture are volume-based. Measuring cylinders and beakers were used to obtain accurate amounts of each constituent material.

After the dry mix and the binder have been thoroughly and uniformly mixed, the final mixture is poured into the wooden mould for the test sample, and the procedure is repeated using the cast iron mould for the actual brake pad composite.

**Table 1** Sample composition of dry composite mixtures

Samples	Particle size	Constituents	% Composition
Sample A Dry Mix	300 $\mu\text{m}$	Aluminium dross	60
		Coconut	30
		Carbon black	5
		Metal chips	5
Sample B Dry Mix	300 $\mu\text{m}$	Aluminium dross	60
		Oil bean	30
		Carbon black	5
		Metal chips	5
Sample C Dry Mix	212 $\mu\text{m}$	Aluminium dross	60
		Coconut	30
		Carbon black	5
		Metal chips	5
Sample D Dry Mix	212 $\mu\text{m}$	Aluminium dross	60
		Oil bean	30
		Carbon black	5
		Metal chips	5



**Table 2** Mixing ratio between binder and dry mixture

Samples	Constituents	% Composition
A	Sample A Dry Mix	30
	Binder	70
B	Sample B Dry Mix	30
	Binder	70
C	Sample C Dry Mix	30
	Binder	70
D	Sample D Dry Mix	30
	Binder	70

**Mould preparation, pouring and setting**

The mould used for creating the samples to be tested is a square box 15 × 15 cm with a depth of 1.5 cm. This box was used to create two samples by partitioning it with a 1.5 × 15 cm divider with a depth of 1.5 cm. This gave the final size of the space to contain a sample as 6.75 × 15 cm with a depth of 1.5 cm. The box was made of small pieces of wood joined together by nails.

Petroleum jelly was used as a release agent to facilitate the easy retrieval of the resulting product from the mould without structural damage by preventing the adhesion of the product and the mould. The inside surfaces of the mould where the composite would be poured were coated with petroleum jelly before the final mixture was carried out. After mixing the epoxy with the dry powder composite, the mixture was quickly poured into the prepared mould to prevent solidification in the mixing bowl. See Fig. 8. This



**Fig. 8** Pouring of the mixture into mould boxes and produced samples

process was repeated for the four different samples, and each sample was labelled for identification purposes, as all the samples had the same physical appearance.

The mixture was allowed to take the shape of the mould and solidify appropriately before any further activity was carried out. The actual brake pad for the automobile was developed by pouring a similar mixing ratio of the samples into a machined mould. The machining process and the developed brake pads for the automobile are shown in the [Appendix](#). Lubricant gel was rubbed around the mould before pouring to ensure easy removal after solidification for 48 h. A manual hand press was designed to allow for compaction of the mould as shown in the [Appendix](#). The process was repeated after cleaning to mould other samples.

#### ***Removal from mould and preparation for testing***

After solidification, the newly formed composite material had to be detached from the mould. As there was no shrinkage and no draft in the mould design, it proved to be more difficult, and the mould had to be removed by removing the nails forming the joints from the adjacent pieces of wood. This yielded the four desired samples without any physical or structural damage, as shown in Fig. 8. The produced samples were then cut into smaller sizes using a hack saw and filed to regular shapes and sizes using a hand file. These smaller samples were used to carry out the necessary tests to gauge the product's performance.

#### ***Characterization of produced brake pad samples***

##### *(a) Test for specific gravity*

Specific gravity is the ratio of the densities of a material and a reference material, usually water. For a stated volume, it is the ratio of their masses. Materials used in this experiment include a graduated measuring cylinder, beaker, distilled water and digital scale.

##### *Procedure*

The empty beaker was weighed as ( $W_1$ ). The sample was placed in the empty beaker and weighed ( $W_2$ ). With the sample still in the beaker, water was added to a certain point so that the sample was completely immersed and weighed ( $W_3$ ). Then the beaker was emptied of its contents and filled up to the same point used when the sample was immersed and weighed.

$$\text{Specific gravity (SG)} = \frac{W_2 - W_1}{(W_4 - W_1) - (W_3 - W_2)} \quad (1)$$

##### *(b) Test for water absorptivity*

Water absorption is simply the amount of water a material absorbs when immersed in it over some time. It is the ratio of the mass of water absorbed to that of the material when dry, expressed in percentage (%). The ASTM 2010 standard was followed in determining the moisture content.

##### *Procedure*

The selected samples are placed in an oven to dry at 105°C. The dry samples are weighed on the digital scale ( $W_1$ ). The samples are entirely immersed in room-temperature water for 24 h. At the end of the stated time, the samples are gently removed from the water, and surface moisture is removed by wiping them with a clean cloth. The saturated sample is weighed on the digital scale ( $W_2$ ).

$$\text{Water absorption} = (W_2 - W_1)/W_1 * 100\% \quad (2)$$

(c) *Test for hardness*

The hardness of a material is the ability of that material to offer resistance to or withstand penetration when a load is applied (it is simply resistance to deformation). Vickers hardness test was carried out using a Qualitest Vickers hardness tester with a diamond indenter.

Procedure

The material to be tested is placed in the hardness tester beneath the diamond indenter, usually a square-based right pyramid with opposite faces at an angle of 136°. The desired load is applied (1–100 kgf). For this experiment, loads of 3, 30 and 100 kgf were applied. On removing the load, the two diagonals in the crevice created by the load are measured microscopically, and the surface area of the indentation is calculated. The hardness number is obtained by dividing the applied load by the indentation area. The hardness is reported in form 300HV20, implying a Vickers hardness of 300 gotten when the load was 20 kgf.

(d) *Test for compressive strength*

This test is carried out to determine the material's strength during compression, its resistance to compression and under what compressive force the material will fail. The experiment uses a Universal Testing Machine and compression pads.

Procedure

Keep the material to be tested in place between the compression pads and switch on the UTM.

Ensure the drag and leading indicators are in contact, then choose your desired range of loads. Activate the motor that drives the pump by pushing the stated button. Slowly move the head control leftwards until the material fails. Note the load at which the material fails, turn off the machine and unload the material.

(e) *Test for thermal conductivity*

Thermal conductivity is simply the ability of a material to conduct heat. It is the amount of heat that flows per unit of time through a unit cross-sectional area when there is a temperature gradient. The apparatus used was a Hot Disk™ Thermal Constants Analyser, as demonstrated in Fig. 9, that employs the transient plane source (TPS) method that allows for measuring the thermal conductivity of more complex and non-traditional

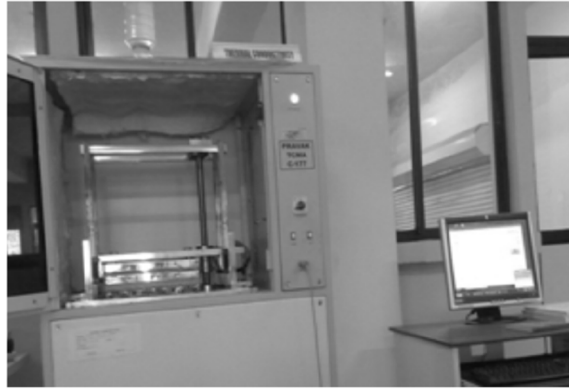


**Fig. 9** Experimental set up and thermal conductivity apparatus

materials. The procedure of this research relates well with the work of Philip and Fagbenle [76].

#### Procedure

The sensor, which was used for both transient heating and the measuring temperature, was of a double-spiral shape made of nickel foil, and was sandwiched by two Kapton (polyimide film) insulator sheets. The sensor remained sandwiched between two sample pieces, with each sample having a surface facing the sensor. Visual inspection confirmed that the sensor was not adjacent to air gaps or cracks on the sample surface to ensure good thermal contact. The experiments were conducted at ambient temperature and with no forced convection. The test was carried out by passing a steady electrical current enough to increase the sensor's temperature (which doubles as a heat source and temperature sensor). The temperature rise was documented as time-dependent. Thermal conductivity ( $k$ ) is given by the Eq. 3.

$$q = kA \frac{T_1 - T_2}{L} \quad (3)$$

where  $k$  = thermal conductivity of the material,  $\Delta T = T_1 - T_2$  is the temperature difference,  $A$  = surface area,  $L$  = thickness,  $q$  = rate of heat transferred

#### (f) SEM/EDX (scanning electron microscope with energy-dispersive X-ray spectroscopy)

A JEOL 7600F Scanning Electron Microscope (SEM) is used to produce a magnified image of a sample by utilizing a focused electron beam. The beam is run along the sample surface in a defined pattern, and the image is created due to electrons coming out of the sample. Unlike the light microscope, where glass lenses focus light photons, in SEMs, electromagnets focus electrons. The quality and type of image produced are a function of the electron beam's interaction with the sample. The SEM creates microscopic ( $10^{-6}$  m) and nanoscopic ( $10^{-9}$  m) images. It has a magnification range of  $\times 10$  to  $\times 300,000$ . Some of the criteria used to describe the image produced by the microscope are briefly explained below:

A scale bar is usually indicated on the SEM image. It indicates the size of the materials shown in the image. WD, or working distance, measures how far apart your sample surface (top face) is from the end of the pole where the electrons emanate (base of the SEM column). Shorter WD results in an electron beam of smaller diameter at the sample surface. HV is the accelerating voltage for electrons measured in kV or keV. The voltage difference between the filament and the anode accelerates the electron beam. A higher kV will result in a beam with higher penetration power into the sample. Magnification is simply enlarging an image or a part of that image. In a SEM, this is obtained by reducing the area being scanned.

EDX is a microanalysis technique that involves identifying which chemical elements constitute a sample under consideration and also studies element atom arrangement. When the beam interacts with the sample, there is an emission of X-rays whose energy is unique to the elements that constitute the sample. An energy-dispersive detector picks up these X-ray signals. They are presented as intensity (number of X-rays) against energy, where the energy shows the elements contained, and the intensity reveals their concentrations. Siegbahn notation is used, where the first part is the element (Mg, Ca, Na), the second part is the ionized electron shell that produced the X-ray (K, L, M) and the third part is the relative intensity of the line within the shells (in decreasing order of intensity:  $\alpha$ ,  $\beta$  and  $\gamma$ ).

#### Procedure

The samples were pulverized by grinding, and each weighed 20 g. Since the materials were not conductive, they were coated with a thin conductive film (coating materials were Au, Pt, Pd, their alloys and carbon). With the SEM left on, the sample chamber was kept under a vacuum to give electrons an uninterrupted path to the sample. The VENT button was long pressed until it flashed and clicked; it kept flashing till the chamber was at atmospheric pressure, indicated by the button turning orange. The door was opened. Hand gloves were used to avoid contaminating the chamber. The doors were slid open, and the sample holder was removed from its position to load the sample. The holder possesses screws to hold the sample in place. These screws were removed to replace the blank sample with the pulverized sample to be tested. The screws were tightened back in place; the holder was placed back in the chamber then the doors closed. While the doors are shut, the chamber is returned to vacuum with the aid of a pump which removes the gases from the chamber bringing the internal pressure to about  $1.3 \times 10^{-9}$  bar. This vacuum state was indicated by the EVAC button turning green. After 5 min, the electron beam was powered on, enabling pictures to be taken. The SEM's computer and the microscope software were powered on. After that, the automatic contrast and brightness button was pushed, enabling the fixed sample to be viewed. Desired magnification was obtained using the magnification X and Y knobs. Pictures were taken, named and saved once desired brightness and contrast were attained. The electron beam was turned off by pushing the green ON button. The chamber was returned to atmospheric pressure with the aid of the VENT button.

#### (g) *Experimental procedures for abrasive wear test*

The wear test is used to determine how much material is removed from the surface of solid objects due to mechanical motion. Wear is typically comparable to material loss brought on by mechanical interactions between two surfaces that are loaded and sliding. This is a typical

occurrence that takes place when two surface-contact objects rub against one another. This causes wear or material displacement between the two rubbing objects [53].

Abrasion wear tests were performed using the Tr-50 Dry Abrasion Tester by ASTM G65 test standards [4]. The wear testing machine was carried out using the following steps on pin-on-disc as shown in the [Appendix](#). The method is dry wear testing.

The specimen is mounted in the tool holder, and a standard load is exerted against it such that its face makes contact with the turning rubber wheel. The silica sand is allowed to flow freely via the hopper's nozzle and into the space between the specimen and the rubber wheel. Three bodies are abraded in the scenario created by the rotating wheel, a chlorobutyl rubber tire, freely flowing silica sand and the specimen. Using a lever arm and a controlled flow of grit, this test specimen is forced against the rotating wheel at a set force. The contact face travels in the direction of the sand flow due to the wheel's rotation. The abrasive particle size, shape, hardness, normal load, amount of stress the particle places on the surface, and frequency of contact will all affect how severe the abrasive wear is. Operators can test the setup under various load-sling speeds, sliding distances and abrasive particle sizes. Test sample weight loss reveals wear resistance. Volume loss will be reduced in materials with higher abrasion resistance.

$$\Delta w = w_a - w_b \quad (4)$$

where  $\Delta w$  = weight loss of the sample

$w_a$  = weight of the sample before the test

$w_b$  = weight of the sample after the test

The specimen's volume loss ( $\Delta V$ ) is calculated as shown in Eq. 4.

$$\Delta V = \frac{(w_a - w_b)}{\rho} \times 1000 \quad (5)$$

where  $\rho$  = experimental density of the sample

The specimen's specific wear rate ( $W_s$ ) is computed in the way described in Eq. 5

$$w_s = \frac{\Delta V}{F_n \times S_s} \quad (6)$$

where  $S_s$  = sliding distance (mm),

$F_n$  = normal load (N)

$$\text{wear resistance} = \frac{\text{sliding distance (S)}}{(V_{\text{loss}} \times 1000)} \quad (7)$$

## Results and discussion

The results obtained in line with the objectives of this research and using the methodology outlined in "[Materials and methods](#)" are presented in this section. This study was conducted to obtain an asbestos-free material for brake pads to replace commercial brake pads. As such, a comparative analysis was carried out between the produced samples and an existing brake pad to determine which sample was used yielded the most desirable results. All the produced samples have the same mixing ratios as



shown in “[Materials and methods](#)” and Table 3; the differentiating factor is the type of natural fibre reinforcement and the particle size of the constituents.

### Specific gravity

Table 4 shows the result of the specific gravity tests carried out, where water was used as the reference material.  $W_1$  through  $W_4$  measured in kilograms (kg).

From the specific gravity results, the samples with smaller particle sizes of 212  $\mu\text{m}$  (C & D) have lower specific gravity and, as a result, lower density than those with larger particle sizes of 300  $\mu\text{m}$  (A & B). For both particle sizes, oil bean stalk reinforced composites (B & D) had lower specific gravity and density than the coconut-reinforced composites (A & C), i.e. (B<A & D<C). This implies that coconut shell is a slightly denser material than oil beanstalk. When compared to the commercial brake pad, the highest SG of the samples (Sample A; 1.257) was less than the SG of the commercial pad (Sample E; 2.081).

This variation in specific gravity results from different mass densities of the sample, an elemental composition such as metals in the matrix, and bonds formed at the atomic level or packing structure of the material. The lower specific gravities of the samples indicate that a lighter material would be obtained for the same volume or geometry when compared to the commercial brake pad. These values correspond to test values obtained by Asotah, W., & Adeleke, A [12]., who investigated using corn husks as filler material in brake pads and obtained a specific gravity of 1.301, while the commercial brake pad used had a specific gravity value of 1.32. Also, Lawal et al. [60] utilized sawdust as the base material to manufacture an asbestos-free brake pad. Three samples were created with different particle sizes and had specific gravity values of 1.91, 1.85 and 1.82, respectively, whereas the commercial brake pad used had a specific gravity of 1.89.

### Water absorption test

Table 5 shows the result of the water absorptivity test carried out on the sample. The experiment was carried out over 24 h.

Sample C was the smallest porous sample and the only sample with a better water absorption rate than the reference sample (sample E). Its percentage composition and unique elemental makeup prevent water penetration. The results of this test indicate that the materials can adapt to conditions such as heavy downpours or water-filled ditches and potholes which automobile motion is often subjected to, and sample C is predicted to adapt the most. At the end of the 24-h period, the commercial brake pad (sample E)

**Table 3** Sample compositions

Sample	Constituents
A	Epoxy matrix with 300 $\mu\text{m}$ particle size and coconut shell reinforcement
B	Epoxy matrix with 300 $\mu\text{m}$ particle size and oil bean stalk reinforcement
C	Epoxy matrix with 212 $\mu\text{m}$ particle size and coconut shell reinforcement
D	Epoxy matrix with 212 $\mu\text{m}$ particle size and oil bean stalk reinforcement
E	Commercial brake pad

**Table 4** Specific gravities of samples

Sample	$W_1$	$W_2$	$W_3$	$W_4$	Specific gravity
A	0.0457	0.0584	0.0966	0.0940	<b>1.257</b>
B	0.0457	0.0554	0.0955	0.0940	<b>1.183</b>
C	0.0457	0.0553	0.0952	0.0940	<b>1.143</b>
D	0.0457	0.0549	0.0951	0.0940	<b>1.136</b>
E	0.0457	0.0611	0.1020	0.0940	<b>2.081</b>

$$\text{Specific gravity (SG)} = \frac{W_2 - W_1}{(W_4 - W_1) - (W_3 - W_2)}$$

**Table 5** Water absorptivity of samples

Sample	Dry sample weight (kg)	Saturated weight (kg)	Moisture absorbed (kg)	Water absorption (%)
A	0.0126	0.0128	0.0002	<b>1.587</b>
B	0.0084	0.0085	0.0001	<b>1.19</b>
C	0.0105	0.0106	0.0001	<b>0.95</b>
D	0.0092	0.0094	0.0002	<b>2.174</b>
E	0.0194	0.0196	0.0002	<b>1.031</b>

was visually observed to have undergone some form of corrosion (suspected to be on its metallic constituents). A crimson tint appeared in the water where the sample was immersed, suspected to be a result of corrosion. This possible weight loss by corrosion might have offset some of the weight of water truly absorbed. The results of this test agree with Ramanathan et al. [82], who utilized lemon peel in combination with aluminium oxide, iron oxide, epoxy resin and hardener to produce asbestos-free brake pads. The best sample produced had a water absorptivity of 0.96%. Also, Asotah & Adeleke [12] investigated using corn husks as filler material in brake pads to replace asbestos; the best sample had a water absorptivity of 0.91% (Lawal et al. [60] utilized sawdust as the base material to manufacture an asbestos-free brake pad); three samples were created with different particle sizes and had water absorptivity values of 0.63, 1.11 and 2.09%, respectively.

#### Comprehensive strength analysis and Young's modulus of elasticity

The compressive strength of samples A–D in Tables 6, 7, 8, 9 and 10 under 80 KN/m<sup>2</sup> load are (114.67, 110.50, 120.52, 11 and 4.89) MPa while for sample E the commercial brake pad has a compressive strength of 110.70 MPa. The value of the commercial asbestos brake pad is within the value reported by various authors of cognate literature studies such as Asim et al. [11], Artiola et al. [10], Obika et al. [72], Ammar et al. [9], Popoola et al. [77], Friday et al. [40], and Sekunowo et al. [92]. The recommended range for brake materials is 70–125 MPa according to Sekunowo et al. [92]. Therefore, Fig. 10 shows the comparison of the developed materials for brake pads and other brake pads from the literature to show their conformity to the recommended range of compressive strength. Samples A–D are within the recommended range and compete favourably with the

**Table 6** Comprehensive test of sample A

Sample A											
$\sigma_3 = 80\text{kN/m}^2$				$\sigma_3 = 160\text{kN/m}^2$				$\sigma_3 = 320\text{kN/m}^2$			
Penet (mm)	Load N	Strain $\times 10^{-2}$	Stress $\text{kN/m}^2$	Penet. (mm)	Load N	Strain $\times 10^{-2}$	Stress $\text{kN/m}^2$	Penet. (mm)	Load N	Strain $\times 10^{-2}$	Stress $\text{kN/m}^2$
0	0	0	0	0	0	0	0	0	0	0	0
0.28	4	0.42	3.56	0.30	10	0.42	8.80	0.20	5	0.30	4.40
0.53	28	0.79	24.47	0.55	20	0.78	17.55	0.45	10	0.60	8.80
0.67	48	0.90	41.90	1.15	95	1.45	81.74	0.95	12	1.35	10.40
1.00	72	1.40	62.40	1.50	122	2.15	103.50	1.15	16	1.55	13.93
1.52	108	2.17	93.30	2.10	140	2.60	116.50	2.30	28	1.20	24.20
1.99	134	2.80	114.67	2.40	156	3.50	128.45	2.60	56	3.94	47.50

**Table 7** Comprehensive test of sample B

Sample B											
$\sigma_3 = 80\text{kN/m}^2$				$\sigma_3 = 160\text{kN/m}^2$				$\sigma_3 = 320\text{kN/m}^2$			
Penet (mm)	Load N	Strain $\times 10^{-2}$	Stress $\text{kN/m}^2$	Penet. (mm)	Load N	Strain $\times 10^{-2}$	Stress $\text{kN/m}^2$	Penet. (mm)	Load N	Strain $\times 10^{-2}$	Stress $\text{kN/m}^2$
0	0	0	0	0	0	0	0	0	0	0	0
0.25	4	0.33	3.50	0.30	10	0.40	8.75	0.20	5	0.25	4.20
0.45	30	0.74	24.44	0.50	20	0.80	17.50	0.40	10	0.60	8.40
0.60	45	0.92	41.80	1.00	90	1.40	80.60	0.90	12	1.30	10.20
1.00	74	1.45	62.40	1.50	110	2.20	100.50	1.20	15	1.48	12.40
1.54	110	2.20	93.20	2.20	130	2.60	115.40	2.00	30	1.10	22.30
1.78	130	2.75	110.50	2.44	150	3.60	125.55	2.80	50	3.85	45.37

**Table 8** Comprehensive test of sample C

Sample C											
$\sigma_3 = 80\text{kN/m}^2$				$\sigma_3 = 160\text{kN/m}^2$				$\sigma_3 = 320\text{kN/m}^2$			
Penet (mm)	Load (N)	Strain $\times 10^{-2}$	Stress $\text{kN/m}^2$	Penet. (mm)	Load N	Strain $\times 10^{-2}$	Stress $\text{kN/m}^2$	Penet. (mm)	Load N	Strain $\times 10^{-2}$	Stress $\text{kN/m}^2$
0	0	0	0	0	0	0	0	0	0	0	0
0.10	21	0.12	18.49	0.70	52	0.12	45.79	0.31	6.4	0.39	5.62
0.50	26	0.80	34.31	0.60	40	0.54	47.50	0.45	12.1	0.55	9.18
0.65	42	0.98	40.82	1.10	99	1.62	11.60	0.95	15	1.38	12.24
1.10	69	1.52	68.70	1.60	140	2.85	108.14	1.10	19	1.50	18.88
1.59	98	2.48	97.42	2.09	156	2.82	120.24	2.04	32	1.21	25.10
1.90	114	2.72	120.52	2.70	170	3.94	130.48	2.60	58	3.78	50.45

commercial brake pad. Ruzaidi et al. [87] developed six palm slag composite specimens for brake pads. The specimen with the highest density of  $2.69 \text{ g/cm}^3$  yielded the highest compressive strength of 76 MPa. The compactness of the specimen and the nature of the filler contribute to the compressive strength of the whole material. Obika et al. [72] obtained a compressive strength of 107.3 MPa alongside a density of  $1.73 \text{ g/cm}^3$ .

**Table 9** Comprehensive test of sample D

Sample D											
$\sigma_3 = 80\text{kN/m}^2$				$\sigma_3 = 160\text{kN/m}^2$				$\sigma_3 = 320\text{kN/m}^2$			
Penet (mm)	Load N	Strain $\times 10^{-2}$	Stress $\text{kN/m}^2$	Penet. (mm)	Load N	Strain $\times 10^{-2}$	Stress $\text{kN/m}^2$	Penet. (mm)	Load N	Strain $\times 10^{-2}$	Stress $\text{kN/m}^2$
0	0	0	0	0	0	0	0	0	0	0	0
0.28	4	0.39	3.51	0.32	10	0.44	8.78	0.20	5	0.28	4.40
0.53	28	0.74	24.51	0.53	20	0.74	17.50	0.43	10	0.60	8.78
0.67	48	0.93	41.93	1.02	94	1.42	81.70	0.95	12	1.32	10.44
1.00	72	1.39	62.6	1.55	120	2.15	103.54	1.10	16	1.53	13.89
1.52	108	2.11	93.22	2.03	136	2.62	116.54	2.00	28	1.00	24.00
1.99	134	2.76	114.89	2.55	151	3.54	128.43	2.80	56	3.89	47.46

**Table 10** Comprehensive test of sample E

Sample E											
$\sigma_3 = 80\text{kN/m}^2$				$\sigma_3 = 160\text{kN/m}^2$				$\sigma_3 = 320\text{kN/m}^2$			
Penet (mm)	Load N	Strain $\times 10^{-2}$	Stress $\text{kN/m}^2$	Penet. (mm)	Load N	Strain $\times 10^{-2}$	Stress $\text{kN/m}^2$	Penet. (mm)	Load N	Strain $\times 10^{-2}$	Stress $\text{kN/m}^2$
0	0	0	0	0	0	0	0	0	0	0	0
0.25	4	0.35	3.50	0.30	10	0.40	8.72	0.20	5	0.25	4.20
0.45	30	0.78	24.48	0.50	20	0.70	17.30	0.40	10	0.60	8.46
0.60	45	0.90	41.88	1.00	90	1.40	80.40	0.91	12	1.30	10.40
1.00	74	1.43	62.35	1.50	110	2.20	100.33	1.10	16	1.44	12.41
1.54	110	2.20	93.10	2.10	130	2.60	115.22	2.00	30	1.00	22.10
1.78	130	2.70	110.70	2.44	148	3.58	125.39	2.80	55	3.88	45.31

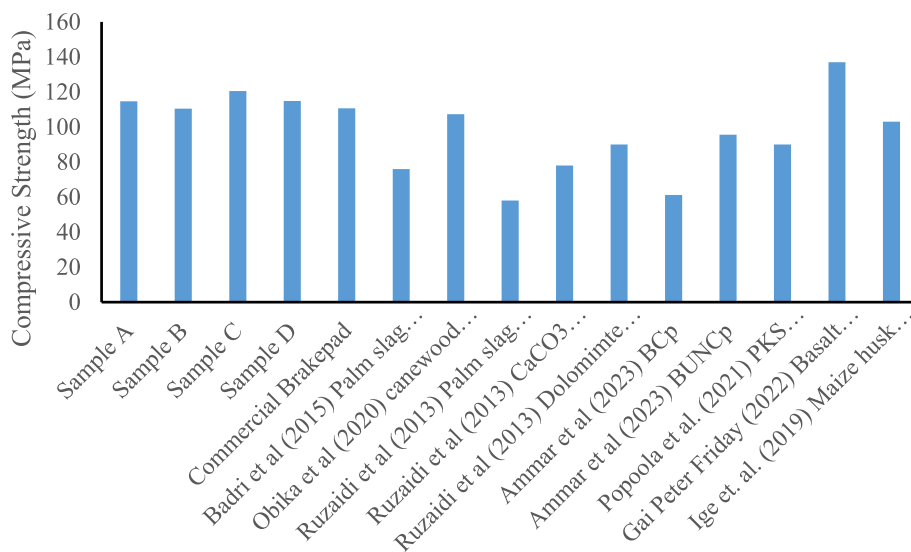


**Fig. 10** Compressive strength of developed brake pad material and existing brake pads

The density compares with commercial brake pads with the range (1.02–2.05) g/cm<sup>3</sup>. They are lighter in weight and thus conform to the standard [73, 83]. Developed samples A–D showed superior compressive strength due to their material makeup employed. The work of the authors showed that pulverized canewood and palm kernel combined well with epoxy resin thereby yielding a good compressive strength and density. Ruzaidi et al. [87] investigated different fillers such as palm slag, CaCO<sub>3</sub>, and dolomite with phenolic as a binder where metal fibre was used as the reinforcement, graphite used as a lubricant, and alumina served as abrasive. The work of the authors showed that dolomite had an outstanding compressive strength of 90 MPa due to the high compactness as posited by the authors. Developed samples still showed high compressive strength due to their composition and compactness. Ammar et al. [9] investigated the influence of natural fibre on the frictional material of brake pads. Banana composite at 30% phenolic resin had a compressive strength of 61.2 MPa while BUNC<sub>p</sub> at 25% phenolic resin had a compressive strength of 95.6 MPa. The authors advocated for the use of natural fibres as it reduces environmental impact and decreases the effect of asbestos which generates a toxic effect on the environment. The developed samples A–D that generated high compressive strength values had natural fibres such as pulverized oil bean stalk and coconut fibres which also contribute as a viable replacement for asbestos commercial brake pads. Popoola et al. [77] used palm kernel shells (PKS), coconut shells (CS), seashells and cowbone as fillers for the production of brake pads. PKS stood out with the compressive strength of 90 MPa and posited that the materials can be well combined to obtain brake pads. The availability of materials such as seashells comes into question as compared with other readily available secondary waste such as PKS and CS. The question on the availability of materials also connects to the work of Gai Peter Friday et al. [40] who developed different basalt-based brake pads with a compressive strength range of 70–137 MPa. Ige et al. [35] developed a brake pad using maize husk and obtained a compressive strength value of 103 MPa which is within the recommended range of compressive strength.

Plotting stress against strain, the slope of the resulting graph will yield Young's modulus of elasticity of the material. For sample A, three sets of values were provided and they produced Young's modulus values of 4398.956kN/m<sup>2</sup> ( $4.398956 \times 10^{-3}$  GPa), 4189.928kN/m<sup>2</sup> ( $4.189928 \times 10^{-3}$  GPa) and 1163.485kN/m<sup>2</sup> ( $1.163485 \times 10^{-3}$  GPa) respectively.

Plotting stress against strain, the slope of the resulting graph will yield Young's modulus of elasticity of the material. For sample B, three sets of values were provided, and they produced Young's modulus values of 4277.02kN/m<sup>2</sup> ( $4.27702 \times 10^{-3}$  GPa), 3976.253kN/m<sup>2</sup> ( $3.976253 \times 10^{-3}$  GPa) and 1128.627kN/m<sup>2</sup> ( $1.128627 \times 10^{-3}$  GPa) respectively.

Plotting stress against strain, the slope of the resulting graph will yield Young's modulus of elasticity of the material. For sample C, three sets of values were provided, and they produced Young's modulus values of 4012.887kN/m<sup>2</sup> ( $4.012887 \times 10^{-3}$  GPa), 2955.38kN/m<sup>2</sup> ( $2.95538 \times 10^{-3}$  GPa) and 1300.971kN/m<sup>2</sup> ( $1.300971 \times 10^{-3}$  GPa) respectively.

Plotting stress against strain, the slope of the resulting graph will yield Young's modulus of elasticity of the material. For sample D, three sets of values were provided, and they produced Young's modulus values of 4480.981kN/m<sup>2</sup> ( $4.480981 \times 10^{-3}$  GPa),

4133.641kN/m<sup>2</sup> ( $4.133641 \times 10^{-3}$  GPa) and 1155.139kN/m<sup>2</sup> ( $1.155139 \times 10^{-3}$  GPa) respectively.

Plotting stress against strain, the slope of the resulting graph will yield Young's modulus of elasticity of the material. For sample E, three sets of values were provided, and they produced Young's modulus values of 4354.651kN/m<sup>2</sup> ( $4.354651 \times 10^{-3}$  GPa), 3974.259kN/m<sup>2</sup> ( $3.974259 \times 10^{-3}$  GPa) and 1110.254kN/m<sup>2</sup> ( $1.110254 \times 10^{-3}$  GPa) respectively.

### Hardness test

Table 11 shows the results of the Vickers hardness test carried out on the samples. Loads of 3, 30 and 100 kgf were used. Hardness is measured in Vickers Pyramid Number (HV), and the applied load determines the number. The resulting unit is kgf/mm<sup>2</sup> or simply HV number as it is the ratio of applied force to the indentation area.

$$HV = F / A \text{ [kgf/mm}^2\text{]}$$

Sample C was the sample with the best values for hardness for all the applied loads of 3, 30 and 100 kgf. Sample C was the only sample with higher hardness than the reference sample (sample E) for all three applied loads. Sample C had hardness values of 19.4HV3, 28.7HV30 and 29.6HV100, while sample E had hardness values of 16.5HV3, 28.4HV30 and 28.2HV100. This implies that for all the applied loads, sample C had the smallest area of indentation or the slightest deformation. It should be noted that all the samples yielded values in the range of the reference sample (sample E) for the three applied loads. This implies that the materials offer similar resistance to local plastic deformation as the commercial brake pad. The test results concord with Atmika et al. [13], Atoyebi et al. [14], Ayilara et al. [15], who developed a composite material for brake lining pad using a phenolic resin matrix and basalt/alumina/shellfish powder reinforcement. Vickers hardness test was performed on the samples according to standard ASTM E-384. The results gave average Vickers Hardness Numbers of 24.18, 25.11, 26.34, 27.21 and 28.83 for the five produced samples, respectively, while the asbestos brake pad had an estimated value of 24.80.

### Thermal conductivity test

Tables 12, 13 and 14 present the thermal conductivities of the four developed brake pad composites and the commercial brake pad. This experiment was carried out on the PASCO's Model TD-8556 Thermal Conductivity Apparatus and the rate of melted ice due to a temperature difference was used to compute the thermal conductivities of the

**Table 11** Hardness test results on samples

Sample ID	HV3	HV30	HV100
Sample A	16.6	26.4	25.5
Sample B	16.4	27.5	28.5
Sample C	19.4	28.7	29.6
Sample D	18.6	26.5	26.7
Sample E	16.5	28.4	28.2



**Table 12** Raw values from the thermal conductivity experiment

Samples	Thickness, h (cm)	Diameter of the ice block before experiment, $d_1$	Diameter of the ice block after experiment, $d_2$	Time to collect melted ice without steam, $t_a$	Mass of the melted ice without steam, $m_{wa}$	Time to collect melted ice with steam, $t_a$	Mass of the melted ice with steam, $m_w$
Sample A	1	7.27	6.91	600	27	420	19
Sample B	1.6	7.39	6.91	600	24	420	17
Sample C	1.6	7.94	7.55	600	27	420	19
Sample D	1.6	7.96	7.51	600	27	420	19
Commercial brake pad	1	6.74	6.053	600	17	420	12

**Table 13** Data and calculations table

Samples	Average diameter, $d_{avg}$ (cm)	Area of the ice surface, A	Rate at which ice melted before steam, $R_a$	Rate at which ice melted after steam, R	Rate at which ice melted due to temperature difference, $R_o$	Thermal conductivity, $calcm/cm^2 s ^\circ C$	Thermal conductivity, W/mK
Sample A	7.09	39.48	0.045	0.04524	$2.4 \times 10^{-4}$	$4.86 \times 10^{-6}$	0.00204
Sample B	7.15	40.15	0.04	0.0405	$5 \times 10^{-4}$	$1.594 \times 10^{-5}$	0.00668
Sample C	7.745	47.11	0.045	0.04524	$2.4 \times 10^{-4}$	$6.521 \times 10^{-6}$	0.00273
Sample D	7.735	46.99	0.045	0.04524	$2.4 \times 10^{-4}$	$6.54 \times 10^{-6}$	0.00274
Commercial brake pad	6.3965	32.13	0.0283	0.0286	$3 \times 10^{-4}$	$7.47 \times 10^{-6}$	0.00313

**Table 14** Thermal conductivities of samples

Samples	Thermal conductivity, $calcm/cm^2 s ^\circ C$	Thermal conductivity, W/mK	Thermal resistivity, Km/ W
Sample A	$4.86 \times 10^{-6}$	0.00204	490.196
Sample B	$1.594 \times 10^{-5}$	0.00668	149.701
Sample C	$6.521 \times 10^{-6}$	0.00273	366.300
Sample D	$6.54 \times 10^{-6}$	0.00274	364.964
Commercial brake pad	$7.47 \times 10^{-6}$	0.00313	319.489

composite samples. A low thermal conductivity is sought out among the developed samples as it is suitable for brake pad applications.

After experimenting with the needed procedures, these values were obtained:

Mass of container = 37.0 g

Time for collecting melted ice without steam,  $t_a = 10 \text{ min} = 600 \text{ s}$

Time for collecting melted ice with steam,  $t_a = 7 \text{ min} = 420 \text{ s}$

Using these:

$D_{avg} = d_1 + d_2 / 2$

$$R_a = m_{wa}/t_a$$

$$R = m_w/t$$

$$R_o = R - R_a$$

$$k = (R_o)(80 \text{ cal/gm}) (h) / (A)(\Delta T).$$

$$\Delta T = \text{Boiling point of water (100 °C at sea level)} - 0^\circ\text{C} = 100^\circ\text{C}$$

From this, the sample with the lowest thermal conductivity value is sample A. However, this sample showed a deformation in the structure during the experiment as it began to melt. Therefore, the most suitable samples are samples C and D, as they gave a very low and suitable thermal conductivity value even when compared to sample E. A low value of thermal conductivity is attributed to a good interfacial bonding between the reinforcement particle and the matrix according to Olabisi et al. [73].

An investigation of the relationship between thermal conductivity and thermal resistivity, as shown in Fig. 11, is necessary to compare both high and low values of both thermal parameters to investigate and establish the flame retardance and suitability of the developed brake pad composites.

**Wear test**

Table 15 presents the results for the specific wear rate and wear resistance of the control commercial brake pad and three developed samples. Sample C has the highest wear resistance while the control sample is quite equivalent to it. This implies that both sample C and the control can withstand progressive volume loss on its surface by sliding, friction and scraping. The material compositions and microstructures account for the wear resistance of brake pads a further implication is that sample C and the control will retain their thickness with distance when compared to samples A and B. The wear resistance is a reflection of the specific wear rate, the reason for the low wear rate of sample C and the control. These further corroborate their wear capacities.

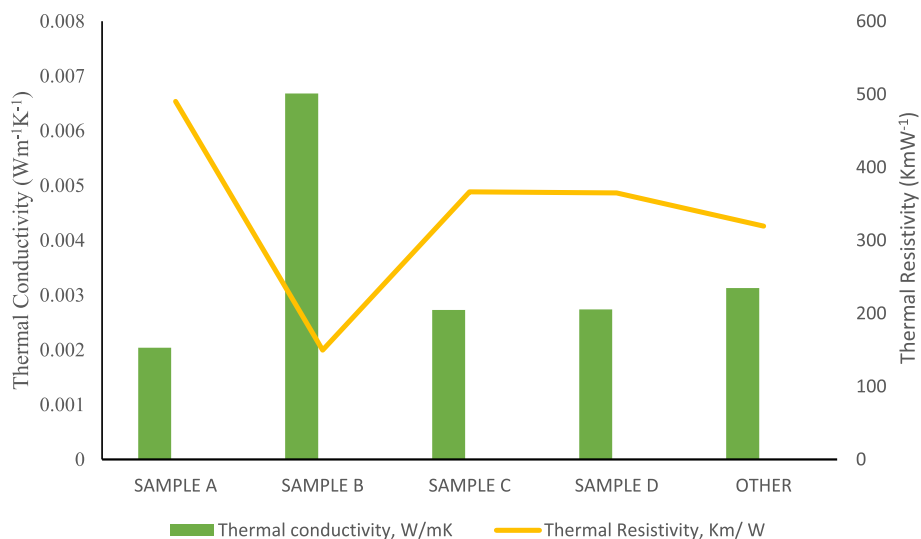


**Fig. 11** Thermal conductivity and thermal resistivity

**Table 15** Results of specific wear rate and wear resistance

S/N	Sample	Initial mass (g) a	Final mass (g) b	Weight loss (g) C=a-b	Volume (ml)	Density d	Sliding distance (mm) S	Vol loss $\Delta V=C/d \times 1000$ mm <sup>3</sup>	Specific wear rate $W_s = \Delta V/F \times S$ (mm <sup>3</sup> /Nm)	Wear resistance (mm/mm <sup>3</sup> )
1	Control	4.91	4.90	0.0093	2.10	2.34	0.39	3.97	1.02	0.098
2	A	11.3	11.33	0.0042	8.98	1.26	0.13	3.33	2.56	0.039
3	B	9.33	9.32	0.0092	7.80	1.19	0.25	7.73	3.09	0.032
4	C	14.21	14.21	0.0084	12.00	1.18	0.71	7.12	1.00	0.099

**Table 16** Summary of average coefficient of friction of brake pad on different surfaces

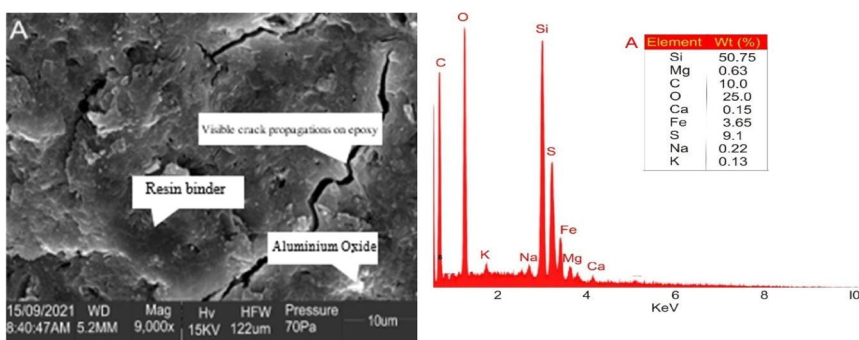
	Wood	Metal	Rubber
Sample A	0.25	0.28	0.59
Sample B	0.15	0.24	0.59
Sample C	0.16	0.19	0.49
Sample D	0.15	0.23	0.62
Sample E: Control	0.98	0.25	0.78

The amount of friction between two surfaces is measured by the coefficient of friction,  $\mu$ . A low coefficient of friction value means that less effort is needed to cause sliding than would be needed if the coefficient of friction were to be high.

Table 16 presents a summary of the average coefficient of friction of the brake pads on different surfaces. The detailed calculation is shown in the Appendix. The brake pads on rubber surfaces will have more slip resistance than wood and metal since they have higher values of COF. Surfaces with high values of  $COF \geq 0.6$  are generally rough and provide a grip for the material over the surface [115]. However, the brake disc in which the brake pad interacts is made of metallic material. The reason for this will be connected to its resistance to combustion despite heat generation on continuous interaction with the brake pad, unlike the rubber and wood surfaces. Sample A is outstanding in its resistance to slip when compared to both the control and other samples due to its higher COF. Most materials in dry conditions have COF that ranges between 0.21 and 0.55 [22]. For tensioning and constant drag applications, where a low tangential force is necessary, a COF of 0.21 (on the low end) is adequate. When you wish to enhance the braking force in static holding applications, high-coefficient materials are frequently the best choice. With a higher coefficient of friction, a strong braking force can be produced with less fluid pressure (lighter pedal pressure).

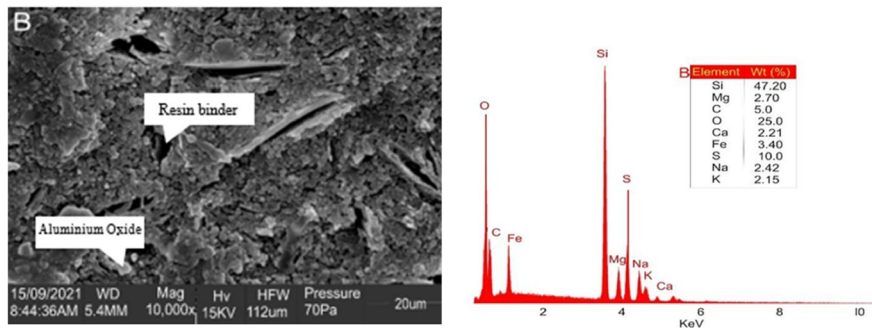
**SEM/EDX analysis**

Figures 12, 13, 14, 15 and 16 show the SEM/EDS analysis used to characterize the advanced brake pad composites to examine the bond formation and determine their compositions (Tables 17, 18, 19, 20 and 21). The micrographs at different magnifications reveal inhomogeneity in their structures, they appeared as flakes, cloudy-oval



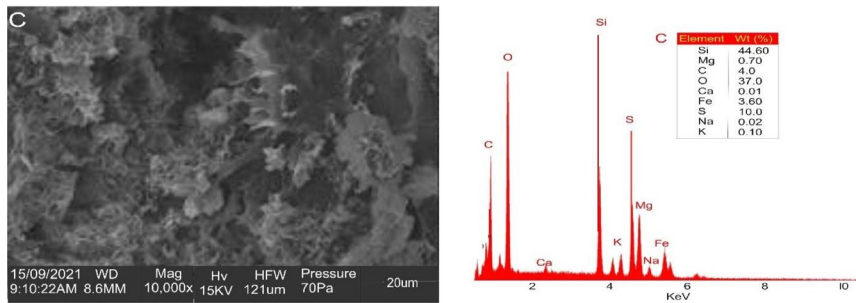
(a) Sample A micrograph @ 9000x (b) EDX graph of Sample A

**Fig. 12** a Sample A micrograph @ x9000. b EDX graph of sample A



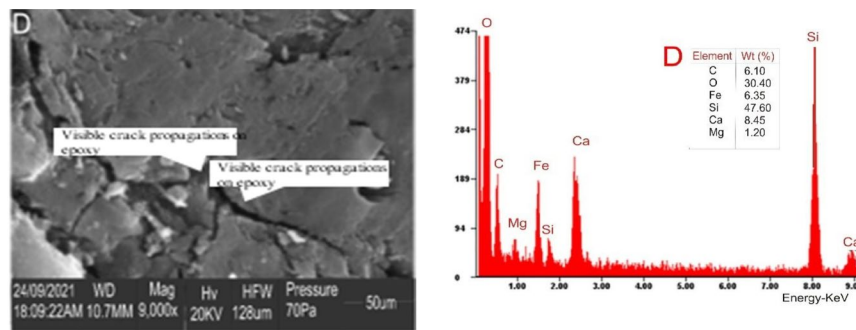
(a) Sample B micrograph @ 20 μm (b) EDX graph of Sample B

Fig. 13 a Sample B micrograph @ 20 μm. b EDX graph of sample B



(a) Sample C micrograph @ 10000x (b) EDX graph of Sample C

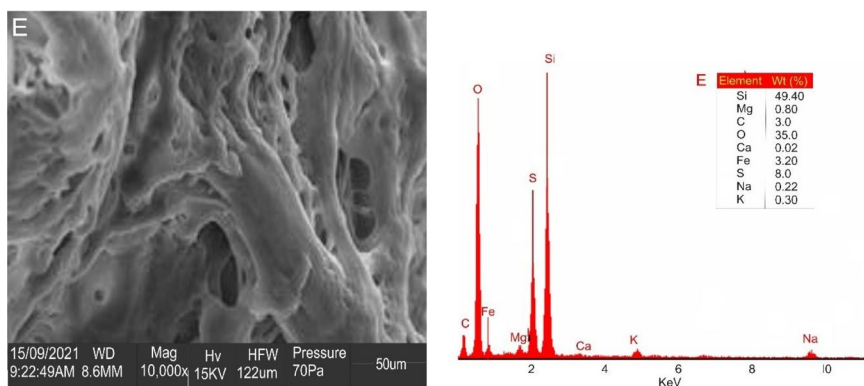
Fig. 14 a Sample C micrograph @ ×10,000. b EDX graph of sample C



(a) Sample D micrograph @ 9000x (b) EDX graph of Sample D

Fig. 15 a Sample D micrograph @ ×9000. b EDX graph of sample D

shapes while the energy-dispersive spectroscopy revealed the presence of the following elements at different proportions as silicon, magnesium, carbon, oxygen, calcium, iron, sulphur, sodium and potassium. The presence of these elements represents the characteristics of individual materials that form the composite. The shiny white spot from the EDS is the MgO phase as maintained by Sekunowo et al. [92] while the dark spots are the well-dispersed FeO. The ash-coloured portion is the high crystalline ceramic



(a) Sample E micrograph @ 10000x (b) EDX graph of Sample E

**Fig. 16** a Sample E micrograph @ ×10,000. b EDX graph of sample E

**Table 17** EDX analysis of sample A

Elements	Si	Mg	C	O	Ca	Fe	S	Na	K
WT (%)	50.75	0.63	10.00	25.00	0.15	3.65	9.10	0.22	0.13

**Table 18** EDX analysis of sample B

Elements	Si	Mg	C	O	Ca	Fe	S	Na	K
WT (%)	47.20	2.70	5.00	25.00	2.21	3.40	10.00	2.42	2.15

**Table 19** EDX analysis of sample C

Elements	Si	Mg	C	O	Ca	Fe	S	Na	K
WT (%)	44.60	0.70	4.00	37.00	0.01	3.60	10.00	0.02	0.10

**Table 20** EDX analysis of sample D

Elements	Si	Mg	C	O	Ca	Fe	S	Na	K
WT (%)	47.60	1.20	6.10	30.40	8.45	6.35	-	-	-

**Table 21** EDX analysis of sample E

Elements	Si	Mg	C	O	Ca	Fe	S	Na	K
WT (%)	49.40	0.80	3.00	35.00	0.02	3.20	8.0	0.22	0.30

compound formed from the mixture of aluminium dross and additives. The micrograph for all the samples also showed that FeO where well dispersed without accumulating at a spot. Microstructure shows a partial adhesion of the particles for sample A, improved adhesion for sample B, good adhesion for sample C similar to commercial sample E, and

good adhesion for sample D; between the base particle and the reinforced particle. Sample C and Sample E had few microvoids, unlike samples A, B and D which had more sized microvoids. SEM was used to analyse the surface morphology of the brake pad materials, and EDX was used to determine the composition of the materials. Figures 12, 13, 14, 15 and 16 illustrate the SEM/EDS analysis utilized in the evaluation of the created brake pad composites to analyse bond formation and determine their compositions. Every sample must conform to the specifications of the specimen chamber to be accommodated, and they are frequently firmly mounted on a specimen support, or “stub,” to hold the sample in place. A 6-in. (15-cm) semiconductor wafer can be examined in all of its sections using a variety of scanning electron microscope types, some of which can be tilted to 450°. Depending on the application, samples will be coated with electrically driven platinum layering, which will either be deposited on the sample by low-vacuum sputtering or high-vacuum evaporation. To maintain an adequate vacuum at the electron gun, the optical electron column is pumped, which results in a short working distance for SEM devices placed in a relatively high-pressure chamber with a short working distance. The high-pressure area surrounding the SEM sample cancels out. The high-pressure zone that surrounds the SEM sample neutralizes the load and greatly amplifies the secondary electron signal’s strength. Because field guns (FEG) can produce high primary luminosity and small spot sizes even at low accelerating potential, low-voltage scanning electron microscopy (SEM) is frequently performed in a FEG-SEM. A resin with a mirror-like finish that can be used with back-drawn electrodes or for quantitative X-ray microanalysis can incorporate biological and material specimens. The energy-dispersive X-ray spectroscopy (EDS) spectra revealed the elemental makeup of the samples, while the micrographs demonstrated the inhomogeneity in the microstructure of the samples as particles emerged in dendritic and oval shapes. O, Si, Al, Mg and Ca were present in sample A, and these elements as well as Fe (iron) were present in samples B, C, D and E. Some of the EDS spectra also showed phases that could not be differentiated, indicating the presence of additional elements in the traces. The dark spots in the microstructure were probably caused by the FeO phase from the mill scale, while the whitish spots were probably the MgO phase from the magnesia. The mullite ( $3\text{Al}_2\text{O}_3 \cdot 2\text{SiO}_2$ ) phases, a highly crystalline ceramic compound made from a bentonite-silica mixture, are most likely responsible for the ash-coloured needle-like portions, while the spinel phase that formed during the samples’ sintering is most likely responsible for the grey and whitish spots. The micrographs in Figs. 12, 13, 14, 15 and 16 demonstrated that there was no obvious agglomeration and that the FeO was evenly distributed throughout the microstructure. The sintering between the mill scale particles and the matrix particles is evident in the microstructures, which also demonstrated good adhesion of the particles.

Sample A was maintained at a pressure of 70 Pa, an accelerating voltage of 15 keV was applied, magnifications of  $\times 8000$ ,  $\times 9000$  and  $\times 10,000$ , working distances of 5.2 and 5.6 mm, horizontal field widths of 114, 122 and 126 m, and scales of 2, 10 and 100 m were utilized in various combinations to produce the micrographs shown below for the SEM analysis. Figure 12 reveals that the peculiar dual-layered structure of the resin film may be to blame for the preferential cracking. As a result of concentrated stress/strain localized near the interface between the amorphous layer and the aluminium substrate, during compressive deformation, the amorphous layer may begin to crack. Another factor



to consider is the significant length of time sample A took in comparison to the other samples to harden. The cracking could be present as a result of impurities in the mixture.

Sample B was maintained at a pressure of 70 Pa, an accelerating voltage of 15 keV was utilized, magnifications of  $\times 9000$  and  $\times 1000$ , working distances of 5.4, 8.3 and 8.6 mm, horizontal field width of 122 m, and scales of 20, 50 and 100 m were used in various combinations to produce the micrographs displayed below for the SEM analysis. Contrarily, Figs. 12 and 13 show the distribution of alumina in the white area and the resin binder in the dark area and a significant concentration of cracks in the microstructure which is a result of the peculiar dual-layered structure of the resin, and sample hardening period. The EDX analysis shows how much Na and K are present in the formulation. Sample C was maintained at a pressure of 70 Pa, an accelerating voltage of 15 keV was utilized, magnifications of  $\times 8000$ ,  $\times 9000$  and  $\times 1000$ , a working distance of 8.6 mm, horizontal field widths of 121 and 122 m and scales of 20 and 50 m were utilized in various combinations to produce the micrographs shown below for the SEM analysis. The EDS analysis of this sample reveals that silicon has a very high percentage composition. Figures 12 and 14 indicate that it has a pozzolanic impact, according to the results. Silicon sand, for example, will react with calcium hydroxide, often known as hydrated calcium. Any substance that exhibits a favourable reaction with hydrated calcium demonstrates that the material has a pozzolanic effect. An even distribution of the dry mixture with the resin is also evident. There is little to no visible variability with regard to white and dark spot concentrations which reflect the homogenous mixture of the dry material composition with the resin. Sample D was maintained at a pressure of 70 Pa, an accelerating voltage of 20 keV was applied, magnifications of  $\times 8000$ ,  $\times 9000$  and  $\times 1000$ , working distances of 10.5, 10.6 and 10.7 mm, horizontal field width of 128 m and scales of 20 and 50 m were used to create the micrographs displayed below for the SEM analysis. In this sample, Figures 15 and 16, the elemental composition is revealed by the EDS, which includes oxygen, carbon, silicon, potassium, magnesium and aluminium, to name a few. The presence of aluminium indicates the existence of aluminium dross, calcium and the presence of aluminium as a binder. Based on the potassium content in the sample, it can be concluded that the sample has a strong binding capacity and can form strong bonds with the base material, which is aluminium dross. Figures 14 and 15 also show cracks for the 212  $\mu\text{m}$  particle size and oil beanstalk reinforcement and significant displacement of alumina in the white area and the resin binder in the dark area. The sample hardening period is a factor in the concentration of cracks in the microstructure. Sample E was maintained at a pressure of 70 Pa, an accelerating voltage of 15 keV was applied, magnifications of  $\times 8000$ ,  $\times 9000$  and  $\times 1000$ , a working distance of 8.6 mm, horizontal field widths of 105, 121 and 122 m, and scales of 50 and 100 m were used to create the micrographs displayed below for the SEM analysis. Using SEM, the crystal morphologies of the generated samples can be seen. According to the SEM study, microstructures of coconut fibre in sample C displayed a uniform distribution of abrasive, solid lubricant, binder and friction modifier in the aluminium matrix. Finally, it can be said that the structures displayed an uneven distribution of the elements, which contributed to the inconsistent outcomes. Different particle or element sizes and weights are also contributors to the distribution's heterogeneity. EDS was also used to analyse the materials. The EDS spectrum revealed the presence of silicon, magnesium, carbon, oxygen, calcium,

iron, sulphur, sodium and potassium, as well as other elemental components. The EDS picture result demonstrates the elemental composition of the samples. As corroborated by Agunsoye et al. [6], the SEM micrograph reveals that the composition of the composite material is slightly heterogeneous due to the varying constituent material combinations (2016). The elemental composition by weight percentage reveals that the samples contain eco-friendly elements. All elements present make a unique contribution to the final product, and their behaviour is discernible at low, moderate and high temperatures or rates of the chemical reaction occurring in the final product. From Figs. 12, 13, 14, 15 and 16, the crystal morphologies of the developed samples were imaged using SEM. The samples were also examined using EDS. The EDS spectrum revealed the presence of silicon, magnesium, carbon, oxygen, calcium, iron, sulphur, sodium, potassium and other elemental constituents. The EDS image result is evidence of the elemental makeup of the samples. The SEM micrograph indicates that the composition is slightly heterogeneous due to different constituent material combinations for the composite material, as supported by Agunsoye et al. [6] and Akil et al. [7]. The elemental composition by percentage weight shows eco-friendly elements in the samples. All elements present have a specific contribution to the final product. Their behaviour can be evident at mild, moderate and elevated temperatures or the rate of the chemical reaction taking place in the product.

### Summary of results

Properties	Highest value	Lowest value	Control (commercial brake pad)
Specific gravity	<i>1.257 (Sample A)</i>	1.136 (Sample D)	<b>2.081</b>
Water absorptivity	1.19 (Sample B)	<i>0.95 (Sample C)</i>	1.03
Compressive Strength (MPa)	<i>120.5 (Sample C)</i>	114.89 (Sample D)	110.7
Hardness Value (HV100)	<i>29.6 (Sample C)</i>	25.5 (Sample A)	28.5
Thermal Conductivity (W/mK)	0.00668 (Sample B)	<i>0.00204 (Sample A)</i>	0.00313
Wear resistance (mm/mm <sup>3</sup> )	<i>0.099 (Sample C)</i>	0.032 (Sample B)	0.098
Specific wear rate (mm <sup>3</sup> /Nm)	3.09 (Sample B)	<i>1.00 (Sample C)</i>	1.02
COF (wood surface)	<i>0.25 (Sample A)</i>	0.15 (Sample D)	<b>0.98</b>
COF (metal surface)	<i>0.28 (Sample A)</i>	0.19 (Sample C)	0.25
COF (rubber surface)	<i>0.62 (Sample D)</i>	0.49 (Sample C)	<b>0.78</b>

The italicized data indicates the preferred value in terms of application while bold data of the control shows the preferred value when compared to the developed samples. From the summary table, sample C (212  $\mu\text{m}$ : coconut shell powder) appeared most with five desirable values in water absorptivity 0.95, compressive strength 120.5 MPa, hardness value 29.6 HV100, wear resistance 0.099 mm/mm<sup>3</sup>, specific wear rate 1.00 mm<sup>3</sup>/Nm. The chemical composition, particle sizes and good interfacial bonding of the microstructure are responsible for the outstanding values. Next close to it is sample A (300  $\mu\text{m}$ : coconut shell powder) with four desirable values in specific gravity 1.257, thermal conductivity 0.00204 W/mK, COF (wood surface) 0.25, COF (metal surface) 0.28. Sample D (212

µm: oil bean powder) only appeared outstanding in one negligible COF (rubber surface). Sample B (300 µm: oil bean powder) did not appear remarkable in any of the properties. These objectives were met as the eco-friendly brake pads were manufactured from natural fibres. The mechanical, chemical and thermal testing were conducted on these brake pads and the results of these tests were compared to those of existing brake pads.

From the results of these tests discussed, it can be summarized that:

- The composite materials are free of harmful elements and compounds, as shown by the elemental analysis, and have a low sulphur content;
- The developed samples had low water absorption rates, which is desirable, and sample C had the best rate at 0.95 percent after 24 h;
- The specific gravities of the developed samples were significantly lower than that of the control sample;
- The specific gravity of the developed samples was significantly lower among the developed samples, sample D had the lowest specific gravity (1.136), while sample A had the highest specific gravity (1.257); all developed samples exhibited very similar hardness values when compared to the commercial brake pad, but only sample C exhibited superior hardness for all three applied loads.
- Sample C had Vickers hardness values of 19.4HV3, 28.7HV30 and 29.8HV100;
- The developed samples all displayed similar values for Young's modulus of elasticity when compared with the commercial brake pad, indicating materials with a similar elasticity, whereas sample A and sample D demonstrated superior elasticity in all three sets of stress and strain values provided;
- The coconut shell-reinforced composites are denser than their oil bean counterparts and this should be taken into consideration

The developed brake pads performed better than the existing commercial brake pads. The chemical tests demonstrated that the natural fibres adhered effectively to the epoxy matrix, and the thermal and mechanical testing yielded results comparable to those of commercial brake pads. Thus, they can be utilized as an acceptable substitute for asbestos brake pads.

## Conclusions

An asbestos-free brake pad was developed from aluminium dross, epoxy resin/hardener, carbon black, oilbean powder, coconut shell powder and pulverized metal chips using the compressive mould method. Analysis of the produced composite brake pad was done, and the results were compared to imported brake pads purchased in Nigeria.

The produced composite was found to be somewhat suitable for use as brake pads for cars based on a comparison of output. There was good interfacial bonding for the samples but coconut shell powder was outstanding as it increased from 212 to 300 µm which is evident in both samples C and A. Specific conclusion for each test is given as follows:

- Compressive strength, hardness and specific gravity of the developed brake pad samples were seen to be increasing with increasing the particle size of the pulver-

ized coconut shell from 212 to 300  $\mu\text{m}$ , while the water absorption and wear rate decreased with increasing the particle size of pulverized coconut shell.

- The composite materials are free from harmful elements and compounds as shown by the elemental analysis and have a low sulphur content.
- The developed samples had low water absorption rates which are desirable and sample C had the best rate at 0.95% after 24 h.
- The specific gravities of the developed samples were considerably lower than that of the commercial brake pad indicating a lighter and less dense material. Of the developed samples, sample D had the lowest specific gravity (1.136), while sample A had the highest specific gravity (1.257).
- All the developed samples gave very similar hardness values when compared with the commercial brake pad but only sample C provided superior hardness for all three applied loads. Sample C had Vickers hardness numbers of 19.4HV3, 28.7HV30 and 29.6HV100.
- The compressive strength of the developed samples is within the recommended standard and is within the value of the commercial brake pad, sample E. Sample C has the highest compressive strength integrity. The coconut shell-reinforced composites are denser than their oil bean counterparts and this should be taken into consideration based on the application required. The developed brake pads fared favourably when compared with the existing commercial brake pads.
- The chemical tests showed the natural fibres bonded well in the epoxy matrix, and the thermal and mechanical tests showed comparable results with the values obtained from the commercial brake pads. They can be used as a suitable replacement for asbestos brake pads.
- Coconut shells and oil bean stalk natural fibres serve as good fillers for the development of brake pads. The results obtained for the coconut shell particles compared favourably with that of the commercial brake pad.

The results of this research indicate that coconut shell particles combine well with aluminium dross, metal chips, graphite and resin-hardener binders. Sample C and sample A can be effectively used as a replacement for asbestos in brake pad manufacture.

## Nomenclature

Symbol	Name	Unit
$\rho$	Density	$\text{Kg}/\text{m}^3$
$k$	Thermal conductivity	$\text{Wm}^{-1}\text{K}^{-1}$
$\Delta T$	Temperature difference	K
$q$	Rate of heat transferred	W
$A$	Indentation area	$\text{mm}^2$
$F$	Applied force	N
$W$	Weight	$\text{Kgms}^{-2}$
$L$	Thickness	m

### Abbreviations

EDX	Energy-dispersive X-ray spectroscopy
HV	Heating value
SG	Specific gravity
SEM	Scanning electron microscope
PKS	Palm kernel shell
CS	Coconut shell
COF	Coefficient of friction

### Supplementary Information

The online version contains supplementary material available at <https://doi.org/10.1186/s44147-023-00345-y>.

#### Additional file 1.

### Acknowledgements

The management of Covenant University is hereby appreciated for continued publication support. The Department of Material Science and Engineering, Obafemi Awolowo University is appreciated for making available their equipment for this research.

### Authors' contributions

The authors confirm their contribution to the paper as follows: study conception and design: JOD conceptualization of idea, writing, analysing and editing. IPO substantive revision of the manuscript. PBA test sample design and characterization, writing and analysing. SOO revision of the manuscript. LKT revision of the manuscript. OAO title revision and substantive revision of the manuscript. EmOO tribological data acquisition and characterization. EnOO solid work CAD design of brake pad mould and holder, produced the actual brake pad. JOU solidwork CAD design of brake pad mould and holder, produced the actual brake pad. All other authors reviewed the results and approved the final version of the manuscript.

### Funding

No funding was received for this work. We confirm that we have given due consideration to the protection of intellectual property associated with this work and that there are no impediments to publication, including the timing of publication, with respect to intellectual property.

### Availability of data and materials

The datasets generated during and/or analysed during the current study are available from the corresponding author upon reasonable request.

### Declarations

#### Competing interests

The authors declare that they have no competing interests.

Received: 25 June 2023 Accepted: 17 December 2023

Published online: 01 March 2024

### References

1. Abdel-Shafy HI, Mansour MS (2018) Solid waste issue: sources, composition, disposal, recycling, and valorization. *Egypt J Pet* 27(4):1275–1290
2. Abhulimen EA, Orumwense FFO (2017) Characterization and development of asbestos free brake pad, using snail shell and rubber seed husk. *Afr J Eng Res* 5(2):24–34
3. Adegbeye MJ, Reddy PRK, Obaisi AI, Elghandour MMMY, Oyebamiji KJ, Salem AZM et al (2020) Sustainable agriculture options for production, greenhouse gasses and pollution alleviation, and nutrient recycling in emerging and transitional nations-an overview. *J Clean Prod* 242:118319
4. Agarwal G, Patnaik A, Sharma RK (2013) Parametric optimization and three-body abrasive wear behavior of sic filled chopped glass fiber reinforced epoxy composites. *Int J Compos Mater* 3(2):32–38
5. Agarwal J, Sahoo S, Mohanty S, Nayak SK (2020) Progress of novel techniques for lightweight automobile applications through innovative eco-friendly composite materials: a review. *J Thermoplast Compos Mater* 33(7):978–1013
6. Agunsoye JO, Bello SA, Bello L, Idehenre MM (2016) Assessment of mechanical and wear properties of epoxy based hybrid composites. *Adv Prod Eng Manag* 11(1):5–14
7. Akil H, Omar MF, Mazuki AM, Safiee SZAM, Ishak ZM, Bakar AA (2011) Kenaf fiber reinforced composites: A review. *Mater Des* 32(8-9):4107–4121
8. Akincioğlu G, Akincioğlu S, Öktem H, Uygur İ (2020) Wear response of non-asbestos brake pad composites reinforced with walnut shell dust. *J Aust Ceram Soc* 56:1061–1072
9. Ammar Z, Ibrahim H, Adly M, Sarris I, Mehanny S (2023) Influence of Natural Fiber Content on the Frictional Material of Brake Pads—A Review. *J Compos Sci* 7(2):72
10. Artiola JF (2019) Industrial waste and municipal solid waste treatment and disposal. In: *Environmental and Pollution Science*. Academic Press, pp 377–391

11. Asim M, Saba N, Jawaid M, Nasir M (2018) Potential of natural fiber/biomass filler-reinforced polymer composites in aerospace applications. In: Sustainable composites for aerospace applications. Woodhead Publishing, pp 253–268
12. Asotah W, Adeleke A (2017) Development of asbestos free brake pads using corn husks. *Leonardo Electron J Pract Technol* 31:129–144
13. Atmika IKA, Subagia IDGA, Surata IW, Sutantra IN (2019) Hardness and wear rate of basalt/alumina/shellfish powder reinforced phenolic resin matrix hybrid composite brake lining pads. In: IOP Conference Series: Materials Science and Engineering (Vol. 539, No. 1, p. 012012). IOP Publishing
14. Atoyebi OD, Osuolale OM, Ibitogbe EM (2019) Strength evaluation of *Cocos nucifera* fibre reinforced concrete. *J Eng Appl Sci* 14(21):8061–8066
15. Ayilara MS, Olanrewaju OS, Babalola OO, Odeyemi O (2020) Waste management through composting: challenges and potentials. *Sustainability* 12(11):4456
16. Ayodele TR, Alao MA, Ogunjuyigbe ASO (2018) Recyclable resources from municipal solid waste: assessment of its energy, economic and environmental benefits in Nigeria. *Resour Conserv Recycl* 134:165–173
17. Badri M, Arief DS, Prayitno A (2015) Compressive strength and wear behavior of palm slag composites using various percentage weight of materials content. *Proceedings of Ocean, Mechanical and Aerospace—science and engineering* (November), 1–4
18. Bai W, Roy A, Sun R, Silberschmidt WV (2019) Enhanced machinability of SiC-reinforced metal-matrix composite with hybrid turning. *J Mater Process Technol* 268:149–161
19. Barile C, Casavola C, De Cillis F (2019) Mechanical comparison of new composite materials for aerospace applications. *Compos Part B* 162:122–128
20. Bashar D-A, Peter MB, Joseph M (2012) Material Selection and Production of a Cold-worked Composite Brake Pad. *World J Eng Pure Appl Sci* 2(3):96
21. Bourmaud A, Beaugrand J, Shah DU, Placet V, Baley C (2018) Towards the design of high-performance plant fibre composites. *Prog Mater Sci* 97:347–408
22. Branham T (2022) Brake pads and the coefficient of friction. [VIDEO] Brake Pads and the Coefficient of Friction ([wcbraham.com](http://wcbraham.com))
23. Chauhan V, Kärki T, Varis J (2019) Review of natural fiber-reinforced engineering plastic composites, their applications in the transportation sector, and processing techniques. *J Thermoplast Compos Mater*:0892705719889095
24. Chen G, Wang X, Li J, Yan B, Wang Y, Wu X et al (2019) Environmental, energy, and economic analysis of integrated treatment of municipal solid waste and sewage sludge: a case study in China. *Sci Total Environ* 647:1433–1443
25. Clyne TW, Hull D (2019) An introduction to composite materials. Cambridge University Press
26. Cousins DS, Suzuki Y, Murray RE, Samaniuk JR, Stebner AP (2019) Recycling glass fiber thermoplastic composites from wind turbine blades. *J Clean Prod* 209:1252–1263
27. Das S, Lee SH, Kumar P, Kim KH, Lee SS, Bhattacharya SS (2019) Solid waste management: scope and the challenge of sustainability. *J Clean Prod* 228:658–678
28. Dilshad S, Kalair AR, Khan N (2020) Review of carbon dioxide (CO<sub>2</sub>) based heating and cooling technologies: Past, present, and future outlook. *Int J Energy Res* 44(3):1408–1463
29. Dirisu JO, Fayomi OSI, Oyedepo SO, Jolayemi KJ, Moboluwarin DM (2019a) Critical evaluation of aluminium dross composites and other potential building ceiling materials. *Procedia Manuf* 35:1205–1210
30. Dirisu JO, Oyedepo SO, Fayomi O (2019b) The effect of pulverized oil bean (*Pentaclethra Macrophylla* Benth.) stalk additive on the thermo-mechanical properties and microstructure of aluminium dross composite for building ceilings applications. *Int J Mech Prod Eng Res Dev* 10:2249–6890 ISSN (E): 2249–8001, ISSN (P)
31. Dirisu JO, Fayomi OSI, Oyedepo SO, Udoye NE (2021) Asbestos-free aluminium dross brake pad: a mini review. In: IOP Conference Series: Materials Science and Engineering (Vol. 1107, No. 1, p. 012034). IOP Publishing
32. Duarte JMRMB (2018) Composite panels subjected to multi-impacts at different energy levels (Doctoral dissertation, Universidade de Coimbra)
33. Duque-Acevedo M, Belmonte-Urena LJ, Cortés-García FJ, Camacho-Ferre F (2020) Agricultural waste: review of the evolution, approaches and perspectives on alternative uses. *Glob Ecol Conserv* 22:e00902
34. Durowaye S, Sekunowo O, Lawal G (2020) Physical and mechanical characterisation of asbestos-free particulate ceramic matrix composites. *Eskişehir Tech Univ J Sci Technol A-Appl Sci Eng* 21(4):562–574
35. Ige EO, Inambao LF, Adewumi AG (2019) Biomass-based composites for brake pads: a review. *Int J Mech Eng Technol* 10(3)
36. Elakhame ZU, Olotu OO, Abiodun YO, Akubueze EU, Akinsanya OO, Kaffo PO, Oladele OE (2017) Production of asbestos free brake pad using periwinkle shell as filler material. *Int J Sci Eng Res* 8(6):1728–1735.
37. Elbeshbishy E, Okoye F (2019) Improper disposal of household hazardous waste: landfill/municipal wastewater treatment plant. *Municipal Solid Waste Manag*
38. Ethaib S (2019) Solid waste situation in Thi-Qar governorate. In: IOP Conference Series: Materials Science and Engineering (Vol. 584, No. 1, p. 012023). IOP Publishing
39. Fazzo L, Minichilli F, Santoro M, Ceccarini A, Della Seta M, Bianchi F et al (2017) Hazardous waste and health impact: a systematic review of the scientific literature. *Environ Health* 16(1):1–11
40. Friday GP (2022) Physico-mechanical properties of basalt-based brake pad as alternative to ceramics brake pad. *Saudi J Eng Technol* 7(1):16–33
41. Ghazali CMR, Kamarudin H, Jamaludin SB, Al Bakri AM, Liyana J (2013) Mechanical properties and morphology of palm slag, calcium carbonate, and dolomite filler in brake pad composites. *Appl Mech Mater* 313:174–178
42. Gireesh CH, Prasad KD, Ramji K, Vinay PV (2018) Mechanical characterization of aluminium metal matrix composite reinforced with aloe vera powder. *Mater Today: Proc* 5(2):3289–3297
43. Gopinath A, Senthilkumar M, Babu A (2018) Evaluation of mechanical properties and microstructure of polyester and epoxy resin matrices reinforced with jute, E-glass and coconut fiber. *Mater Today: Proc* 5(9):20092–20103

44. Grennfelt P, Englyrd A, Forsius M, Hov Ø, Rodhe H, Cowling E (2020) Acid rain and air pollution: 50 years of progress in environmental science and policy. *Ambio* 49(4):849–864
45. Günay M, Korkmaz ME, Özmen R (2020) An investigation on braking systems used in railway vehicles. *Eng Sci Technol an Int* 23(2):421–431
46. Gurram P, Komakula SA, Kumar GV (2019) Design and Analysis of Vented Disc Brake Rotor. *Int J Appl Eng Res* 14(9):2228–2233
47. Hoornweg, D., & Bhada-Tata, P. (2012). What a waste: a global review of solid waste management
48. Ishidi EY, Kolawole EG, Sunmonu KO (2011) Morphology and thermal property of alkaline treated palm kernel nut shell HDPE composite. *J Emerg Trends Eng Appl Sci (JETEAS)* 2(2):346–350
49. Jang H, Ko KH, Kim SJ, Basch RH, Fash JW (2004) The effect of metal fibers on the friction performance of automotive brake friction materials. *Wear* 256(3-4):406–414
50. Agunsoye JO, Bello SA, Bamgibaiye AA, Odunmosu KA, Akinboye IO (2017) Recycled ceramic composite for automobile brake pad application. *J Res Phys* 39(1):35–46 (2018)
51. Jouhara H, Czajczyńska D, Ghazal H, Krzyżyńska R, Anguilano L, Reynolds AJ, Spencer N (2017) Municipal waste management systems for domestic use. *Energy* 139:485–506
52. Jouyandeh M, Paran SMR, Jannesari A, Puglia D, Saeb MR (2019) Protocol for nonisothermal cure analysis of thermoset composites. *Prog Org Coat* 131:333–339
53. Juan RS, Kurniawan C, Marbun J, Simamora P (2020) Mechanical properties of brake pad composite made from candlenut shell and coconut shell. *J Phys Conf Ser* 1428(1):012018 IOP Publishing
54. Kaza, Silpa; Yao, Lisa C.; Bhada-Tata, Perinaz; Van Woerden, Frank. 2018. What a Waste 2.0: A Global Snapshot of Solid Waste Management to 2050
55. Koh R, Madsen B (2018) Strength failure criteria analysis for a flax fibre reinforced composite. *Mech Mater* 124:26–32
56. Krishna RS, Mishra J, Meher S, Das SK, Mustakim SM, Singh SK (2020) Industrial solid waste management through sustainable green technology: case study insights from steel and mining industry in Keonjhar, India. *Mater Today: Proc* 33:5243–5249
57. Kumar K, Davim JP (eds) (2018) *Composites and Advanced Materials for Industrial Applications*. IGI Global
58. Kumar VV, Kumaran SS (2019) Friction material composite: types of brake friction material formulations and effects of various ingredients on brake performance—a review. *Mater Res Express* 6(8):082005
59. Kuzina E, Cherkas A, Rimshin V (2018) Technical aspects of using composite materials for strengthening constructions. *IOP Conf Ser Mater Sci Eng* 365(3):032053 IOP Publishing
60. Lawal SS, Bala KC, Alegbede AT (2017) Development and production of brake pad from sawdust composite. *Leonardo J Sci* 30:47–56
61. Li J, Xiao F, Zhang L, Amirkhanian SN (2019) Life cycle assessment and life cycle cost analysis of recycled solid waste materials in highway pavement: a review. *J Clean Prod* 233:1182–1206
62. Liu Y, Xie J, Wu N, Wang L, Ma Y, Tong J (2019) Influence of silane treatment on the mechanical, tribological, and morphological properties of corn stalk fiber reinforced polymer composites. *Tribol Int* 131:398–405
63. Lu H, Sidortsov R (2019) Sorting out a problem: a co-production approach to household waste management in Shanghai, China. *Waste Manag* 95:271–277
64. Malav LC, Yadav KK, Gupta N, Kumar S, Sharma GK, Krishnan S et al (2020) A review on municipal solid waste as a renewable source for waste-to-energy project in India: current practices, challenges, and future opportunities. *J Clean Prod* 277:123227
65. Marimuthu KP, Kumar SM, Kumar VR, Govindaraju HK (2019) Characterization of mechanical properties of epoxy reinforced with glass fiber and coconut fiber. *Mater Today: Proc* 16:661–667
66. Moya D, Aldás C, López G, Kaparaju P (2017) Municipal solid waste as a valuable renewable energy resource: a worldwide opportunity of energy recovery by using Waste-To-Energy Technologies. *Energy Procedia* 134:286–295
67. Mwanza BG, Mbohwa C (2017) Drivers to sustainable plastic solid waste recycling: a review. *Procedia Manuf* 8:649–656
68. Nagarajan S, Radhakrishnan S, Kalkura SN, Balme S, Miele P, Bechelany M (2019) Overview of protein-based biopolymers for biomedical application. *Macromol Chem Phys* 220(14):1900126
69. Nagavally RR (2017) Composite materials—history, types, fabrication techniques, advantages, and applications. *Int J Mech Prod Eng* 5(9):82–87
70. Nickels L (2018) Composites driving the auto industry. *Reinf Plast* 62(1):38–39
71. Nwankwo C, Gobo AE, Israel-Cookey C, Abere SA (2020) Effects of hazardous waste discharge from the activities of oil and gas companies in Nigeria. *Cent Asian J Environ Sci Technol Innov* 1:119–129
72. Obika EN, Achebe CH, Chukwunke JL, Ezenwa ON (2020) Effect of cane wood and palm kernel fibre filler on the compressive strength and density of automobile brake pad. *Adv Mech Eng* 12(7):1687814020947611
73. Olabisi AI, Adam AN, Okechukwu OM (2016) Development and assessment of composite brake pad using pulverized cocoa beans shells filler. *Int J Mater Sci Appl* 5(2):66–78
74. Ologunye, O. B., Abdulumuni, B., Fanifosi, J. O., Azeez, N. A., & Akinola, O. J. (2020) Fabrication and performance evaluation of a low-cost electric baking oven. *School of Engineering Technology Annual International Conference*, 1(1): 22-27, 2020. ISSN: 2756-4126
75. Persson L, Karlsson-Vinkhuyzen S, Lai A, Persson Å, Fick S (2017) The globally harmonized system of classification and labelling of chemicals—explaining the legal implementation gap. *Sustainability* 9(12):2176
76. Philip P, Fagbenle L (2014) Design of Lee's disc electrical method for determining thermal conductivity of a poor conductor in the form of a flat disc. *Int J Innov Sci Res* 9(2):335–343
77. Popoola OT, Rabiu AB, Ibrahim HK, Omoniyi PO, Babatunde MA, Muhammed N, Isiaq FO (2021) Production of Automobile Brake Pads from Palm Kernel Shell, Coconut Shell, Seashell, and Cow Bone. *Adeleke Univ J Eng Technol* 4(2):92–101
78. Praveenkumar B, Darius Gnanaraj S (2020) Case studies on the applications of phenolic resin-based composite materials for developing eco-friendly brake pads. *J Inst Eng (India): D* 101(2):327–334



79. Preeti JKR, Thakur M, Suman M, Kumar R (2018) Consequences of pollution in wildlife: A review. *Pharma Innov J* 7:94–102
80. Rajak DK, Pagar DD, Kumar R, Pruncu CI (2019) Recent progress of reinforcement materials: a comprehensive overview of composite materials. *J Mater Res Technol* 8(6):6354–6374
81. Ramakrishnan S, Loganayagan S, Kowshika G, Ramprakash C, Aruneshwaran M (2021) Adobe blocks reinforced with natural fibres: A review. *Mater Today Proc* 45:6493–6499
82. Ramanathan K, Saravanakumar P, Ramkumar S, Pravin KP, Surender SR (2017) Development of asbestos-free brake pads using lemon peel powder. *Int J Innov Res Technol Sci Eng* 6(3):4449–4455
83. Ramlee NA, Jawaid M, Zainudin ES, Yamani SAK (2019) Tensile, physical, and morphological properties of oil palm empty fruit bunch/sugarcane bagasse fibre reinforced phenolic hybrid composites. *J Mater Res Technol* 8(4):3466–3474
84. Rangappa SM, Siengchin S (2019) Lightweight natural fiber composites. *J Appl Agric Sci Technol* 3(2):178
85. Robitschek D (2021) From mechanical to regenerative braking-implications of the transition towards electric mobility on aspects of deceleration and tribological brake additives (Doctoral dissertation, Wien)
86. Rubino F, Nisticò A, Tucci F, Carlone P (2020) Marine application of fiber reinforced composites: a review. *J Mar Sci Eng* 8(1):26
87. Ruzaidi CM, Kamarudin H, Shamsul JB, Al Bakri AM, Rafiza AR (2013) Effect of palm slag filler size on the mechanical and wear properties of brake pad composites. *Adv Sci Lett* 19(1):118–122
88. Sajjan S, Selvaraj DP (2021) A review on polymer matrix composite materials and their applications. *Mater Today: Proc* 47:5493–5498
89. Sajib SH (2021) A Study on the effects of environmental pollution on human life in the riverbank area of Barishal City Corporation (Kirtankhola River)
90. Sanjay MR, Arpitha GR, Yogesha B (2015) Study on mechanical properties of natural-glass fibre reinforced polymer hybrid composites: a review. *Mater Today: Proc* 2(4-5):2959–2967
91. Sanjay MR, Madhu P, Jawaid M, Senthamaraikannan P, Senthil S, Pradeep S (2018) Characterization and properties of natural fiber polymer composites: a comprehensive review. *J Clean Prod* 172:566–581
92. Sekunowo OI, Bolasodun BO, Oyedepo GT, Oluwole JY (2020) Noise Pollution Mitigation Study of Rice Husk-Ash Nanoparticle Reinforced Epoxy Resin Composites. *J Eng Res.* 25(1):29–38.
93. Sheferaw Tensaye (2021) Development of asbestos free brake-pad using banana peel hybrid composite (Doctoral dissertation, ASTU)
94. Shiva Prasad U, Babu AR, Sairaju B, Amirishetty S, Deepak D (2020) Automotive chassis design material selection for road and race vehicles. *J Mech Eng Res Dev, Zibeline international publishing* 43(3):274–282
95. Siakeng R, Jawaid M, Ariffin H, Sapuan SM (2019) Mechanical, dynamic, and thermomechanical properties of coir/ pineapple leaf fiber reinforced polylactic acid hybrid biocomposites. *Polym Compos* 40(5):2000–2011
96. Singh A (2019) Managing the uncertainty problems of municipal solid waste disposal. *J Environ Manag* 240:259–265
97. Solomon, D. G., & Berhan, M. N. (2007). Characterization of friction material formulations for brake pads. In *World Congress on Engineering* 2:2–4
98. Soltes EJ, Elder TJ (2018) Pyrolysis. In: *Organic chemicals from biomass*. CRC Press, pp 63–99
99. Somashekhar TM, Naik P, Nayak V, Rahul S (2018) Study of mechanical properties of coconut shell powder and tamarind shell powder reinforced with epoxy composites. In: *IOP Conference Series: Materials Science and Engineering* 376(1):012105. IOP Publishing
100. Stalin B, Nagaprasad N, Vignesh V, Ravichandran M, Rajini N, Ismail SO, Mohammad F (2020) Evaluation of mechanical, thermal, and water absorption behaviors of Polyalthia longifolia seed reinforced vinyl ester composites. *Carbohydr Polym* 248:116748
101. Subramanian K, Krishnasamy S, Muthukumar C, Siengchin S, Gnaniar K, Kanagaraj A (2021) Tribology of Wood Polymer Composites. In: *Wood Polymer Composites*. Springer, Singapore, pp 179–193
102. Taufan HS, Purwanto P (2018) The management of toxic and hazardous waste materials in the food industry. In *E3S Web of Conferences* (Vol. 73, p. 07020). EDP Sciences
103. Tonk R (2020) Natural fibers for sustainable additive manufacturing: a state of the art review. *Mater Today: Proc* 37:3087–3090
104. Tulebayeva N, Yergobek D, Pestunova G, Mottaeva A, Sapakova Z (2020) Green economy: waste management and recycling methods. In *E3S Web of Conferences* (Vol. 159, p. 01012). EDP Sciences
105. Umoren SA, Solomon MM (2019) Protective polymeric films for industrial substrates: a critical review on past and recent applications with conducting polymers and polymer composites/nanocomposites. *Prog Mater Sci* 104:380–450
106. Upadhyay RK (2020) Markers for global climate change and its impact on social, biological and ecological systems: A review. *Am J Clim Chang* 9(03):159
107. Veal L (2021). United States environmental protection agency
108. VectorMine. Solid waste management steps with processing and disposal outline diagram. Accessed 01/12/2023. <https://vectormine.com/item/solid-waste-management-steps-with-processing-and-disposal-outline-diagram/>
109. Xiao Y, Xu P, Fan H, Baudouin L, Xia W, Bocs S et al (2017) The genome draft of coconut (*Cocos nucifera*). *Gigascience* 6(11):gix095
110. Xue Y, Wang Y (2020) Green electrochemical redox mediation for valuable metal extraction and recycling from industrial waste. *Green Chem* 22(19):6288–6309
111. Yang Y, Boom R, Irion B, van Heerden DJ, Kuiper P, de Wit H (2012) Recycling of composite materials. *Chem Eng Process Process Intensif* 51:53–68
112. Yashas Gowda TG, Sanjay MR, Subrahmanya Bhat K, Madhu P, Senthamaraikannan P, Yogesha B (2018) Polymer matrix-natural fiber composites: an overview. *Cogent Eng* 5(1):1446667
113. Yi, X. S., Du, S., & Zhang, L. (2018). *Composite Materials Engineering*, Volume 2

114. Yuhazri MY, Zulfikar AJ, Ginting A (2020) Fiber reinforced polymer composite as a strengthening of concrete structures: a review. In: IOP Conference Series: Materials Science and Engineering (Vol. 1003, No. 1, p. 012135). IOP Publishing
115. Zhang H (2016) Surface characterization techniques for polyurethane biomaterials. In: Advances in polyurethane biomaterials (pp. 23-73). Woodhead Publishing
116. Zhang Y, Wu J, Xu B (2018) Human health risk assessment of groundwater nitrogen pollution in Jinghui canal irrigation area of the loess region, northwest China. *Environ Earth Sci* 77(7):1–12

### **Publisher's Note**

Springer Nature remains neutral with regard to jurisdictional claims in published maps and institutional affiliations.